Cell Reports

Article

The heme synthesis-export system regulates the tricarboxylic acid cycle flux and oxidative phosphorylation

Graphical abstract

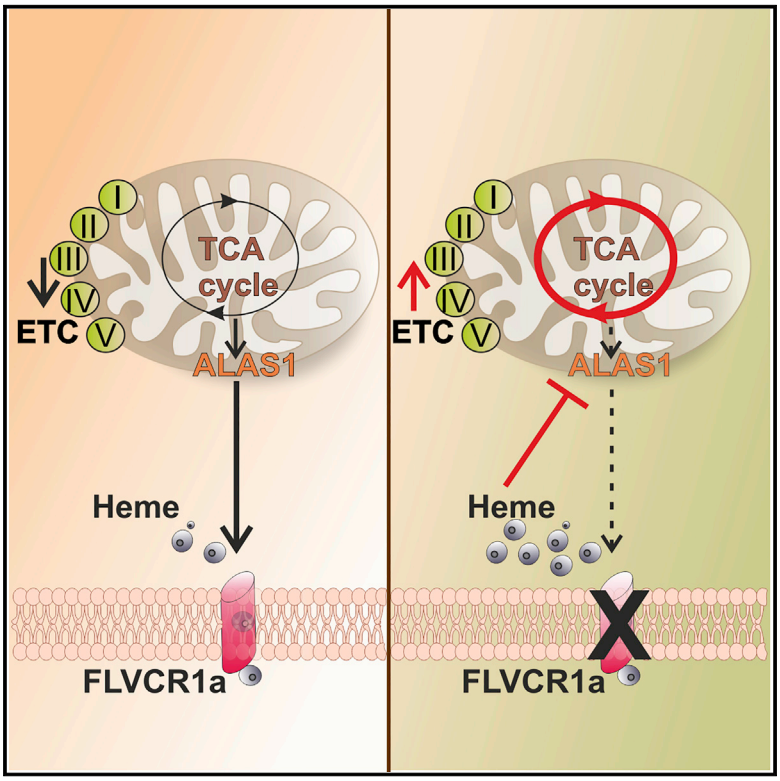

Authors

Veronica Fiorito, Anna Lucia Allocco, Sara Petrillo, ..., Simone Cardaci, Chiara Riganti, Emanuela Tolosano

Correspondence

emanuela.tolosano@unito.it

In brief

High rates of heme synthesis by ALAS1 and heme export by FLVCR1a are commonly observed in proliferating cells. Here, Fiorito et al. illustrate a functional axis between heme synthesis and heme export and show that this system is crucial for controlling the TCA cycle and oxidative phosphorylation.

Highlights

- FLVCR1a sustains heme synthesis limiting the feedback inhibition of heme on ALAS1
- Reduced heme synthesis-export results in the promotion of the TCA cycle and OXPHOS
- The heme synthesis-export system controls oxidative metabolism in proliferating cells

Fiorito et al., 2021, Cell Reports *35*, 109252
June 15, 2021
https://doi.org/10.1016/j.celrep.2021.109252

CellPress

Cell Reports

CellPress
OPEN ACCESS

Article

The heme synthesis-export system regulates the tricarboxylic acid cycle flux and oxidative phosphorylation

Veronica Fiorito,[1] Anna Lucia Allocco,[1] Sara Petrillo,[1] Elena Gazzano,[2] Simone Torretta,[3] Saverio Marchi,[4] Francesca Destefanis,[1] Consiglia Pacelli,[5] Valentina Audrito,[6] Paolo Provero,[1,7] Enzo Medico,[8,9] Deborah Chiabrando,[1] Paolo Ettore Porporato,[1] Carlotta Cancelliere,[9] Alberto Bardelli,[8,9] Livio Trusolino,[8,9] Nazzareno Capitanio,[5] Silvia Deaglio,[6] Fiorella Altruda,[1] Paolo Pinton,[10] Simone Cardaci,[3] Chiara Riganti,[2] and Emanuela Tolosano[1,11,*]

[1]Molecular Biotechnology Center (MBC), Department of Molecular Biotechnology and Health Sciences, University of Torino, Torino, Italy
[2]Department of Oncology, University of Torino, Torino, Italy
[3]Division of Genetics and Cell Biology, San Raffaele Scientific Institute, Milano, Italy
[4]Department of Clinical and Molecular Sciences, Marche Polytechnic University, Ancona, Italy
[5]Department of Clinical and Experimental Medicine, University of Foggia, Foggia, Italy
[6]Immunogenetics Unit, Department of Medical Sciences, University of Torino, Torino, Italy
[7]Center for Omics Sciences, San Raffaele Scientific Institute IRCSS, Milano, Italy
[8]Department of Oncology, University of Torino, Candiolo, TO, Italy
[9]Candiolo Cancer Institute, FPO-IRCCS, Candiolo, TO, Italy
[10]Department of Medical Sciences and Laboratory for Technologies of Advanced Therapies (LTTA), University of Ferrara, Ferrara, Italy
[11]Lead contact
*Correspondence: emanuela.tolosano@unito.it
https://doi.org/10.1016/j.celrep.2021.109252

SUMMARY

Heme is an iron-containing porphyrin of vital importance for cell energetic metabolism. High rates of heme synthesis are commonly observed in proliferating cells. Moreover, the cell-surface heme exporter feline leukemia virus subgroup C receptor 1a (FLVCR1a) is overexpressed in several tumor types. However, the reasons why heme synthesis and export are enhanced in highly proliferating cells remain unknown. Here, we illustrate a functional axis between heme synthesis and heme export: heme efflux through the plasma membrane sustains heme synthesis, and implementation of the two processes down-modulates the tricarboxylic acid (TCA) cycle flux and oxidative phosphorylation. Conversely, inhibition of heme export reduces heme synthesis and promotes the TCA cycle fueling and flux as well as oxidative phosphorylation. These data indicate that the heme synthesis-export system modulates the TCA cycle and oxidative metabolism and provide a mechanistic basis for the observation that both processes are enhanced in cells with high-energy demand.

INTRODUCTION

Heme is an iron-containing porphyrin of vital importance for cells because of its involvement in several biological processes (Chiabrando et al., 2014). Heme can be acquired from dietary sources, but it is also synthetized directly by cells. Heme synthesis consists of eight enzymatic reactions that start in mitochondria with the condensation of succinyl-coenzyme A (CoA) with glycine to form 5-aminolevulinic acid (ALA). This reaction is catalyzed by 5-aminolevulinate synthase (ALAS), the rate-limiting enzyme of the heme synthetic pathway. Two genes encode the ALAS enzyme, *ALAS1*, which is ubiquitously expressed, and *ALAS2*, which is specific for the erythroid lineage. Together with endogenous biosynthesis, cellular heme homeostasis relies on the balanced and coordinated expression/activity of enzymes, transporters, and accessory proteins involved in extracellular heme import, heme incorporation into hemoproteins, heme degradation, and heme export from the cytosol to the extracellular space. This latter activity is mediated by the cell surface feline leukemia virus subgroup C receptor 1a (FLVCR1a), one of the two proteins encoded by the *FLVCR1* gene (Quigley et al., 2004; Khan and Quigley, 2011; Chiabrando et al., 2012).

Heme has profound and complex implications in processes related to cell energy production. Indeed, heme is involved in oxygen transport and has pivotal functions in mitochondria, serving as a cofactor for most of the respiratory chain complexes (Kim et al., 2012) and interacting with the translocases responsible for the ADP/ATP exchange between mitochondria and cytosol (Azuma et al., 2008; Sabová et al., 1993; Giraud et al., 1998). Moreover, heme biosynthesis is considered a cataplerotic pathway for the tricarboxylic acid (TCA) cycle, as the process consumes succinyl-CoA, an intermediate of the TCA cycle (Frezza et al., 2011; Fukuda et al., 2017). Finally, being one of the major cellular iron-consuming activities, heme biosynthesis competes with mitochondrial biogenesis of iron-sulfur (Fe-S) clusters (Barupala et al., 2016), which are crucial cofactors of

electron transport chain (ETC) complexes and of some TCA cycle enzymes.

The control of cell energy metabolism and of nutrient expenditure to sustain energy production is particularly important in cells under conditions of high-energy demand, such as during proliferation. Therefore, it is not surprising that alterations in heme metabolism are frequently observed in cancer (Fiorito et al., 2020). It is commonly assumed that most tumors rely on high heme synthesis by ALAS1. Likewise, increased expression of the heme exporter FLVCR1a has been recently reported. However, the precise mechanisms underpinning enhanced heme synthesis and enhanced heme export in tumors remain substantially unexplored (Russo et al., 2019; Shen et al., 2018; Peng et al., 2018). Experimental evidence suggests that heme synthesis by ALAS1 and heme export by FLVCR1a are two highly coordinated processes (Chiabrando et al., 2012; Vinchi et al., 2014, Doty et al., 2015). However, the two processes have never been studied reciprocally in the context of cancer, and their effect on the global regulation of cell energy metabolism has not been explored in detail.

Here, we document that ALAS1-mediated heme synthesis and FLVCR1a-mediated heme export are intertwined processes and show that the heme synthesis-export axis is crucial for controlling the TCA cycle and oxidative phosphorylation (OXPHOS).

RESULTS

FLVCR1a-mediated heme export sustains heme synthesis

Heme synthesis is mainly controlled by heme itself, through a feedback inhibition on ALAS1 (Zheng et al., 2008; Kubota et al., 2016; Srivastava et al., 1988; Lathrop and Timko, 1993). Therefore, we hypothesized that the promotion of heme export could be a strategy adopted by cells to avoid heme accumulation and, in that way, ensure sustained heme synthesis. To test that hypothesis, we chose as model systems the colorectal cancer (CRC) cell lines Caco2, C80, and SKCO1, in which we silenced *FLVCR1a* using RNA interference (Figure S1).

We focused on CRC because a role for FLVCR1a in intestinal cells was previously demonstrated (Fiorito et al., 2015). Moreover, we found that the *FLVCR1* gene was overexpressed in colorectal tumors, both in humans (Figures S2A and S2B) and in mice (Figure S2C), suggesting an active heme efflux in these cells. The relevance of FLVCR1a for CRC is also supported by the observation that *FLVCR1a*-silenced Caco2 cells proliferated more slowly (Figures S2D and S2E) and displayed a greater extent of basal apoptosis (Figure S2F) than control cells did. Similar to Caco2 cells, *FLVCR1a* silencing also led to increased apoptosis in SKCO1 and C80 cells (Figures S2G and S2H). In line with *in vitro* results, subcutaneous injection of *FLVCR1a*-silenced SKCO1 cells in non-obese diabetic severe combined immunodeficiency (NOD-SCID) gamma (NSG) mice gave rise to smaller tumors than the tumors obtained by the injection of control cells (Figure S2I), confirming the inhibitory effect of *FLVCR1a* knockdown on CRC cell proliferation/survival in an *in vivo* context as well.

To confirm the role of FLVCR1a as a heme exporter and to assess its function in the control of *de novo* synthetized heme, we analyzed the extent and kinetics of heme export and synthesis in CRC cell lines upon *FLVCR1a* silencing. In washout experiments after treatment with the heme analog zinc-mesoporphyrin (ZnMP), *FLVCR1a*-silenced Caco2 cells retained more ZnMP than control cells did (Figure 1A), pointing to FLVCR1a as a crucial mediator of heme efflux in those cells. Moreover, after induction of heme biosynthesis by the heme precursor 5-aminolevulinic acid (5-ALA), *FLVCR1a*-silenced cells experienced a faster and greater increase in the amount of intracellular heme than control cells did. This accumulation was blunted by the heme biosynthesis inhibitor succinylacetone (SA) (Figure 1B), indicating that FLVCR1a prevents the accumulation of *de novo* synthesized heme. We also analyzed the rate of heme synthesis in *FLVCR1a*-silenced Caco2 cells, taking advantage of metabolomic and tracing analyses. Among heme precursors, only 5-ALA could be detected in the experimental conditions of our assays. However, 5-ALA synthesis is the rate-limiting step in heme biosynthesis, reflecting the progress of the entire process. By measuring the intracellular production of 5-ALA, we observed less 5-ALA in *FLVCR1a*-silenced Caco2 cells as compared with that of controls (Figure 1C). In addition, in time-course experiments, *FLVCR1a*-deficient Caco2 cells maintained in medium with uniformly labeled glucose (U-^{13}C-glucose) or glutamine (U-^{13}C-glutamine) showed reduced incorporation of labeled carbons in 5-ALA (Figures 1D and 1E), confirming that ALAS1 activity was reduced in those cells relative to controls. These data strengthen the assumption that the FLVCR1a function is required to sustain heme synthesis. Consistent with data obtained in Caco2 cells, we observed reduced *ALAS1* expression in *FLVCR1a*-silenced SKCO1 and C80 cells (Figure S3). Conversely, *FLVCR1a* overexpression in Caco2 cells resulted in increased *ALAS1* expression (Figure 1F).

These results indicate that, by prompting heme export, FLVCR1a limits the feedback-inhibitory effect of accumulated heme on ALAS1, thus favoring heme production. Hence, the two processes of heme synthesis and heme export define a unique system in which heme export is crucial to sustain heme synthesis.

The heme synthesis-export system controls the OXPHOS rate

Given the strong relationship between heme and cell energy production, we sought to analyze the effect of the heme synthesis-export axis on cellular energetic metabolism. To that end, we evaluated mitochondrial function in *FLVCR1a*-silenced cells.

A significant enhancement in mitochondrial biogenesis was detected upon *FLVCR1a* silencing (Figures 2A, S4A, and S4B), indicating alterations in mitochondrial properties. *FLVCR1a* silencing in Caco2 cells also resulted in increased activity in all the complexes involved in the respiratory chain (Figure 2B), including ATP synthase (Figure 2C). Increased OXPHOS in *FLVCR1a*-silenced cells was supported by additional pieces of evidence, such as increased mitochondrial membrane potential (Figures 2D and S4C), mitochondrial basal calcium levels (Figure 2E), and mitochondrial ability to accumulate calcium upon agonist stimulation (Figure 2F). Moreover, although *FLVCR1a* depletion did not affect total cellular ATP levels (Figure S4D), *FLVCR1a*-silenced cells showed significantly more ATP in the

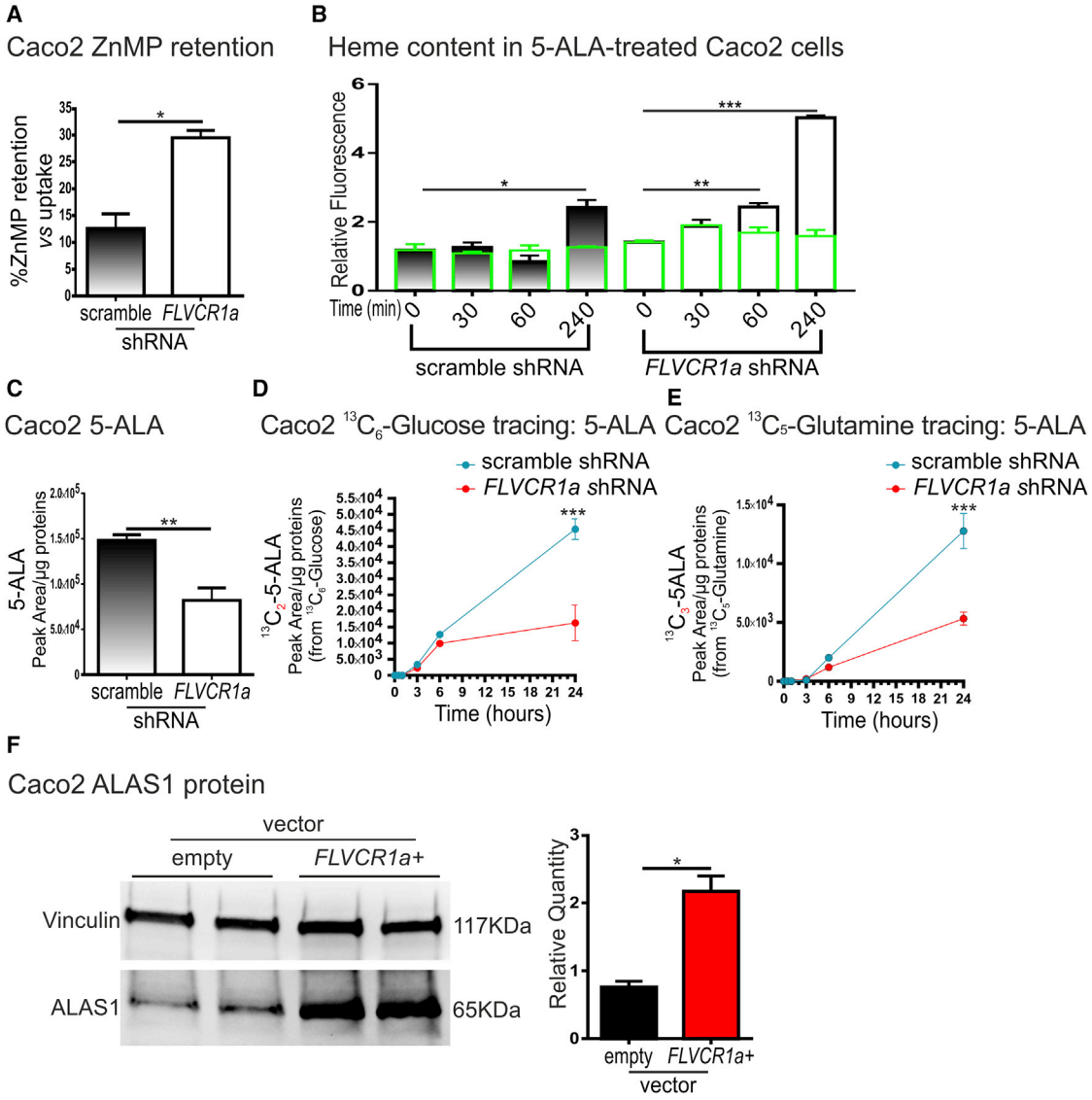

Figure 1. The *FLVCR1a*-mediated heme export sustains heme synthesis

(A) Zinc-mesoporphyrin (ZnMP) retention in Caco2 cells treated with 5 μM ZnMP for 30 min (uptake phase) and fluorometrically analyzed 60 min after removal of ZnMP from the medium (washout phase). The graph shows the percentage of retained ZnMP fluorescence at the end of the washout phase, with respect to the fluorescence detected immediately after the uptake phase. *FLVCR1a*-silenced Caco2 cells are compared with cells expressing a scramble short hairpin RNA (shRNA). Data represent means ± SEM, n = 2. For statistical analyses, an unpaired Student's t test was used. *$p < 0.05$.

(B) Heme content in Caco2 cells treated with 5 mM 5-aminolevulinic acid (5-ALA;black bars and white bars) or with 5 mM 5-ALA + 0.5 mM succinylacetone (SA; green outlined bars) for the indicated time points. *FLVCR1a*-silenced Caco2 cells are compared with cells expressing a scramble shRNA. Values are expressed as relative fluorescence intensity. Data represent means ± SEM, n = 2. For statistical analyses, a two-way analysis of variance was used, followed by the Bonferroni correction for multiple group comparisons. **$p < 0.01$, ***$p < 0.001$.

(C) Intracellular 5-ALA levels. *FLVCR1a*-silenced Caco2 cells are compared with cells expressing a scramble shRNA. Values are expressed as peak area/μg proteins. Data represent means ± SEM of n = 4 wells pooled from two independent experiments. For statistical analyses, an unpaired Student's t test was used. **$p < 0.01$.

(D and E) Accumulation of $^{13}C_2$-5-ALA in cells incubated with U-^{13}C-glucose (D) or of $^{13}C_3$-5-ALA in cells incubated with U-^{13}C-glutamine (E) for the indicated time. *FLVCR1a*-silenced Caco2 cells are compared with cells expressing a scramble shRNA. Values are expressed as peak area/μg proteins. Data represent means ± SEM of n = 4 wells pooled from two independent experiments. For statistical analyses, a two-way analysis of variance was used, followed by the Bonferroni correction for multiple group comparisons. ***$p < 0.001$.

(F) Western blot analysis of ALAS1 expression in Caco2 cells. Cells overexpressing *FLVCR1a* (indicated as *FLVCR1a*$^+$) are compared with cells stably transduced with an empty vector. Vinculin expression is shown as a loading control. Band intensities were measured by densitometry and were normalized to vinculin expression. Densitometry data represent means ± SEM, n = 2. For statistical analyses, an unpaired Student's t test was used. *$p < 0.05$. Data are representative of three independent experiments.

See also Figures S1–S3.

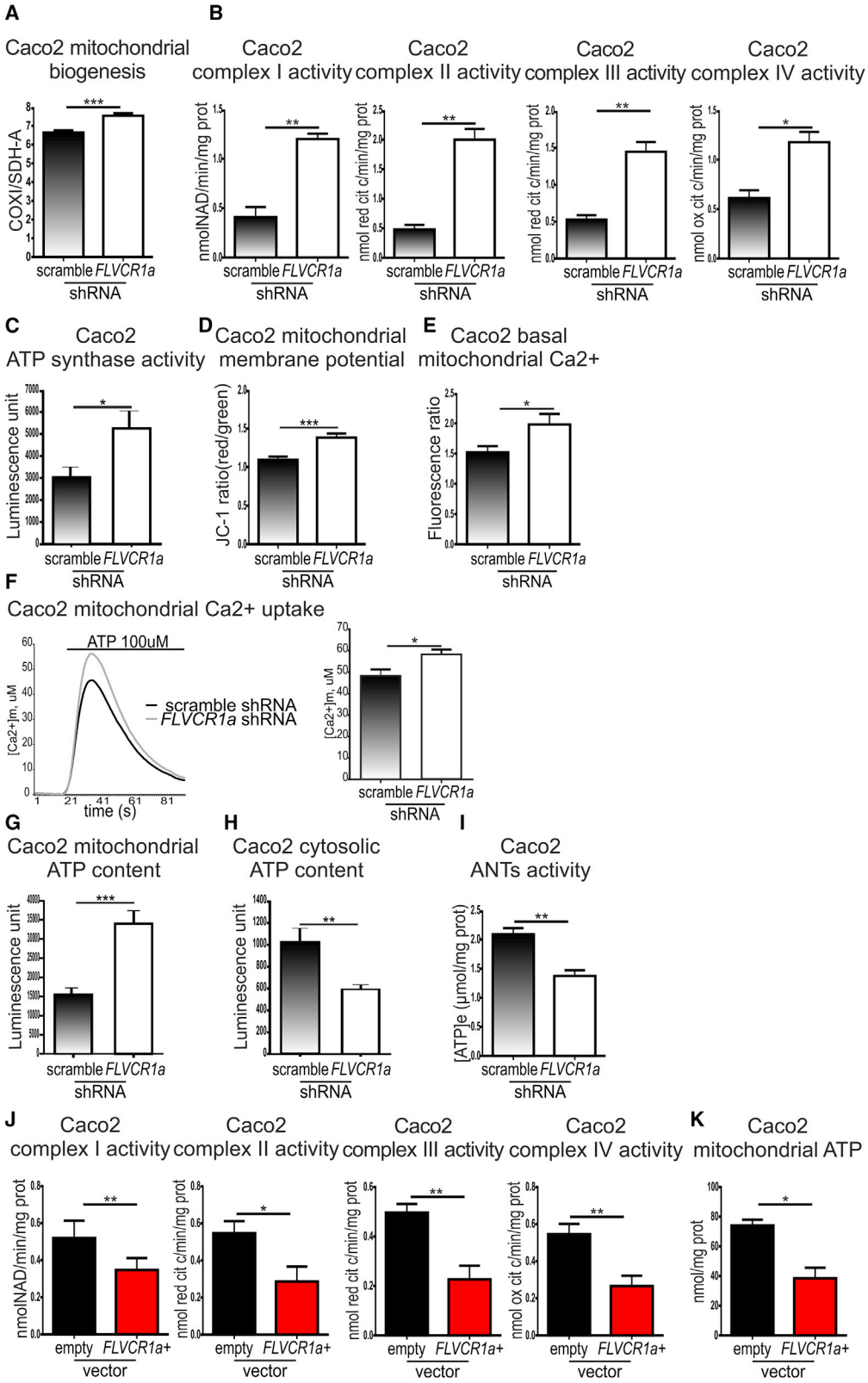

(legend on next page)

mitochondria (Figures 2G, S4E, and S4F) than control cells did. Remarkably, we also measured less ATP in the cytosol of *FLVCR1a*-silenced cells (Figure 2H), indicating ATP retention in the mitochondria. This conclusion is supported by the finding that *FLVCR1a* knockdown led to reduced activity of adenine nucleotide translocases (ANTs) (Figure 2I).

ETC complexes II, III, and IV exploit heme as a cofactor. The role of heme in complex II is still undetermined and likely unrelated to electron transport (Rutter et al., 2010; Kim et al., 2012). Conversely, heme is crucial to the function of complexes III and IV (Kim et al., 2012). The data described above show that *FLVCR1a* silencing is associated with decreased heme synthesis by ALAS1 and with enhanced OXPHOS, suggesting that the amount of heme provided by the residual ALAS1-dependent production is sufficient to sustain the activity of ETC complexes III and IV. In line with that conclusion, we detected reduced complex III and IV activity, as well as decreased ATP production, in *ALAS1*-silenced cells (Figures S4G and S4H), in which heme production is expected to be strongly compromised. Conversely, congruent with that observed in *FLVCR1a*-silenced cells, the activity of complexes I and II was enhanced upon *ALAS1* knockdown (Figure S4G).

The increased ETC complexes activity and mitochondrial ATP levels observed in *FLVCR1a*-silenced Caco2 cells were confirmed in SKCO1 (Figures S4I and S4J) and C80 cells (Figures S4K and S4L). In a complementary perspective, *FLVCR1a*-overexpressing cells showed the opposite phenotype, with a significant reduction in the activity of all the ETC complexes and the mitochondrial ATP levels (Figures 2J and 2K).

Interestingly, the ETC complexes activities returned to baseline levels in *FLVCR1a*-silenced Caco2 cells (Figure S5A) upon short-term serum withdrawal, indicating that the heme synthesis-export system is required to keep down OXPHOS under conditions of serum stimulation. Consistently, after serum starvation in *FLVCR1a*-silenced cells, ATP levels decreased (Figure S5B), and the oxygen consumption rate (OCR) was comparable with that detected in control cells (Figure S5C). Thus, the rate of OXPHOS controlled by the heme synthesis-export system is influenced by environmental conditions. Notably, a surplus of ATP was still present in *FLVCR1a*-silenced cells as compared with that of controls upon serum starvation (Figure S5B), confirming that mitochondrial ATP overload in *FLVCR1a*-silenced cells is partly dependent on mitochondrial ATP retention, rather than solely on increased ATP production.

Figure 2. The heme synthesis-export system controls the OXPHOS rate

(A) Mitochondrial biogenesis expressed as a ratio between the expression of the mitochondrial DNA-encoded protein COX-I (the subunit I of ETC complex IV) and the expression of the nuclear DNA-encoded mitochondrial protein SDH-A (the 70-kDa subunit of ETC complex II). *FLVCR1a*-silenced Caco2 cells are compared with cells expressing a scramble shRNA. Data represent means ± SEM, n = 6. For statistical analyses, an unpaired Student's t test was used. ***p < 0.001.

(B) Activities of the mitochondrial electron transport chain complexes I–IV. *FLVCR1a*-silenced Caco2 cells are compared with cells expressing a scramble shRNA. Results were expressed as nmol of NAD^+/min/mg of mitochondrial protein for complex I, nmol of reduced cytochrome *c*/min/mg of mitochondrial protein for complexes II–III, and nmol of oxidized cytochrome *c*/min/mg of mitochondrial protein for complex IV. Data represent means ± SEM, n = 3. For statistical analyses, an unpaired Student's t test was used. *p < 0.05, **p < 0.01.

(C) ATP measurements using a luciferase-based method in *FLVCR1a*-silenced Caco2 cells compared with cells expressing a scramble shRNA. The accumulation of mitochondrial ATP over the basal ATP levels, upon stimulation of ATP synthesis, is shown. The measure is considered a readout of ATP synthase activity. Data on basal mitochondrial ATP levels (plateau I) and data on mitochondrial ATP levels upon ATP synthesis stimulation with a Ca^{2+}-dependent agent (plateau II) are reported in Figure S4E. The accumulation of ATP was computed as plateau I − plateau II. Data represent means ± SEM of n = 20 coverslips pooled from three independent experiments. For statistical analyses, an unpaired Student's t test was used. *p < 0.05.

(D) Mitochondrial membrane potential measured by the JC-1 fluorescent dye-based method. *FLVCR1a*-silenced Caco2 cells are compared with cells expressing a scramble shRNA. Data represent means ± SEM, n = 6 coverslips pooled from three independent experiments. For statistical analyses, an unpaired Student's t test was used. ***p < 0.001.

(E) Resting mitochondrial calcium levels. *FLVCR1a*-silenced Caco2 cells are compared with cells expressing a scramble shRNA. Data represent means ± SEM of n = 6 coverslips pooled from three independent experiments. For statistical analyses, an unpaired Student's t test was used. *p < 0.05.

(F) Mitochondrial calcium uptake measured as Ca^{2+} responses to an agonist stimulation (100 μM ATP). Representative traces of Ca^{2+} responses are shown. Next, the graph showing quantification of mitochondrial Ca^{2+} from three independent experiments is reported. *FLVCR1a*-silenced Caco2 cells are compared with cells expressing a scramble shRNA. Data represent means ± SEM, n = 14 coverslips pooled from three independent experiments. For statistical analyses, an unpaired Student's t test was used. *p < 0.05.

(G) Basal mitochondrial ATP levels measured using a luciferase probe targeted to the mitochondrial matrix. *FLVCR1a*-silenced Caco2 cells are compared with cells expressing a scramble shRNA. Data are referred to three independent experiments and represent means ± SEM, n = 20 coverslips pooled from three independent experiments. For statistical analyses, an unpaired Student's t test was used. ***p < 0.001.

(H) Basal cytosolic ATP levels measured using a luciferase probe targeted to the cytosol. *FLVCR1a*-silenced Caco2 cells are compared with cells expressing a scramble shRNA. Data represent means ± SEM, n = 20 coverslips pooled from three independent experiments. For statistical analyses, an unpaired Student's t test was used. **p < 0.01.

(I) Adenine nucleotide translocases (ANTs) activity. Results are expressed as μmoles exchanged ATP/mg of mitochondrial proteins. *FLVCR1a*-silenced Caco2 cells are compared with cells expressing a scramble shRNA. Data represent means ± SEM, n = 3. For statistical analyses, an unpaired Student's t test was used. **p < 0.01.

(J) Activities of the mitochondrial electron transport chain complexes I–IV in Caco2 cells overexpressing *FLVCR1a* (indicated as *FLVCR1a*$^+$) compared with cells stably transduced with an empty vector. Results were expressed as nmol NAD^+/min/mg of mitochondrial protein for complex I, nmol of reduced cytochrome *c*/min/mg of mitochondrial protein for complexes II–III, and nmol oxidized cytochrome *c*/min/mg of mitochondrial protein for complex IV. Data represent means ± SEM, n = 3. For statistical analyses, an unpaired Student's t test was used. *p < 0.05, **p < 0.01.

(K) Mitochondrial ATP levels measured by a bioluminescent assay kit in Caco2 cells overexpressing *FLVCR1a* (indicated as *FLVCR1a*$^+$) compared with cells stably transduced with an empty vector. Results are expressed as nmol/mg of mitochondrial proteins. Data represent means ± SEM, n = 3. For statistical analyses, an unpaired Student's t test was used. *p < 0.05.

See also Figures S4 and S5.

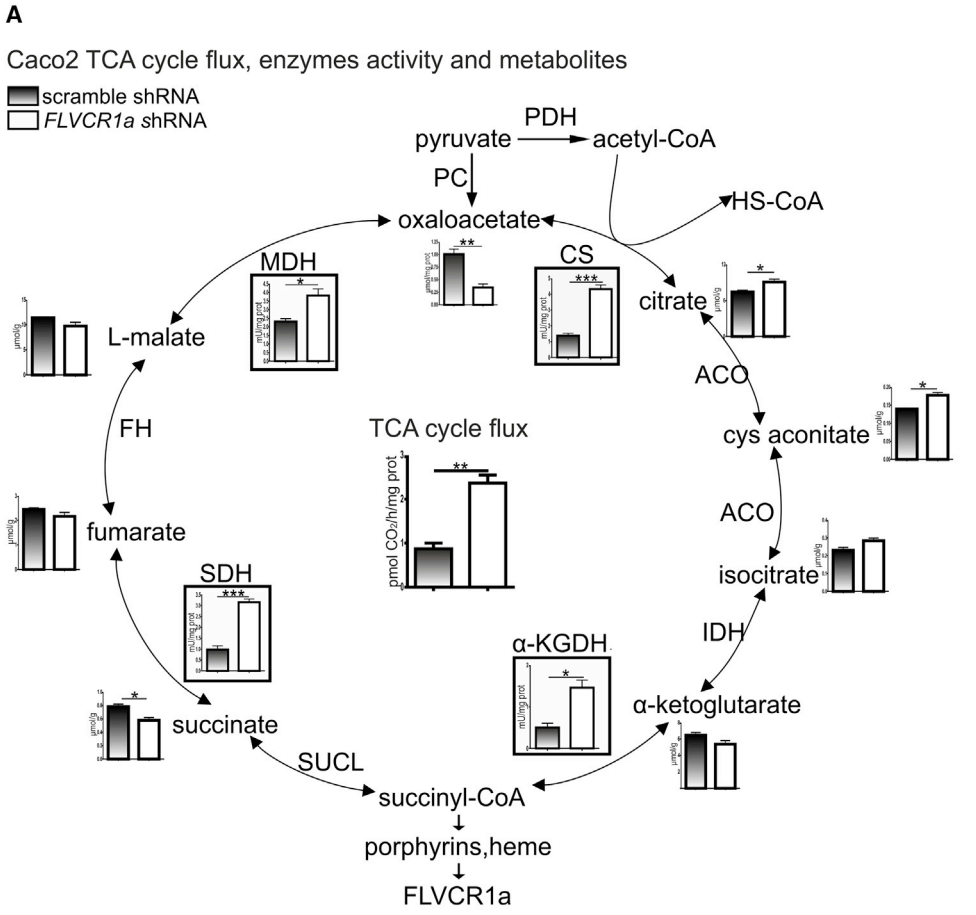

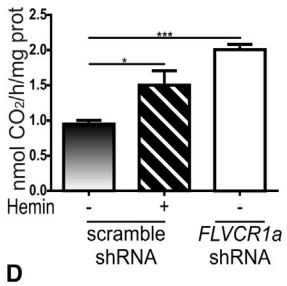

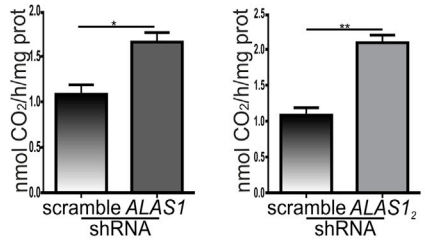

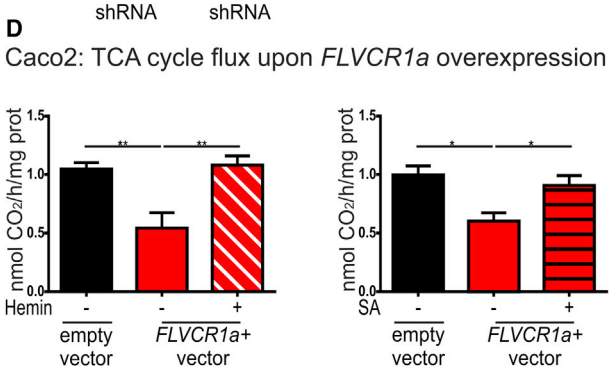

(legend on next page)

Collectively, data indicate that the heme synthesis-export system is required to maintain a low rate of OXPHOS and proper ATP distribution between the mitochondria and the cytosol.

The heme synthesis-export system controls the TCA cycle flux

OXPHOS is sustained by the TCA cycle, and heme synthesis participates in TCA cycle cataplerosis. Accordingly, we examined metabolic differences in the TCA cycle in *FLVCR1a*-deficient versus *FLVCR1a*-proficient Caco2 cells. The total flux of the TCA cycle was significantly upregulated in *FLVCR1a*-silenced cells compared with controls (Figure 3A, see the histogram in the center), and several TCA-cycle enzymes, including citrate synthase, α-ketoglutarate dehydrogenase, succinate dehydrogenase, and malate dehydrogenase (Figure 3A), displayed enhanced activity after *FLVCR1a* knockdown. Increased TCA cycle flux upon *FLVCR1a* silencing was confirmed in SKCO1 and C80 cells (Figures S6A and S6B).

We also evaluated the levels of the TCA-cycle intermediates in *FLVCR1a*-silenced cells, both at steady-state conditions (Figure 3A) and in time-course experiments with cells cultured in medium containing U-^{13}C-glucose or U-^{13}C-glutamine (Figure 4). Under steady-state conditions, complex modulation of TCA-cycle metabolite levels was observed. Indeed, the amount of some intermediates (citrate and *cis*-aconitate) was greater in *FLVCR1a*-silenced cells than it was in controls, in line with the increased activity of the enzymes involved in their production (citrate synthase and aconitase). In contrast, the levels of other intermediates (oxaloacetate and succinate) were reduced (Figure 3A). Time-course experiments revealed that incorporation of labeled carbons from U-^{13}C-glucose in citrate, α-ketoglutarate, and malate was enhanced in *FLVCR1a*-silenced cells, indicating faster consumption of labeled glucose in those cells than in the controls (Figure 4B). Similar results were obtained upon U-^{13}C-glutamine administration (Figure 4C). Interestingly, in *FLVCR1a*-silenced cells maintained in U-^{13}C-glutamine, the appearance of both citrate $^{13}C_4$ and $^{13}C_5$ isotopologues was enhanced (Figure 4C), indicating that *FLVCR1a* silencing stimulates both oxidative and reductive glutamine metabolism. The combined increase of both TCA-cycle flux and reductive carboxylation likely explains the heterogeneous modulation of TCA-cycle intermediates levels detected at steady-state conditions.

The TCA cycle is intended to produce both metabolites and reducing equivalents to support OXPHOS. Interestingly, *FLVCR1a* silencing did not alter the expression of nicotinamide phosphoribosyltransferase (Figure S6C), the main nicotinamide adenine dinucleotide (NAD)-biosynthetic enzymes (NBEs), commonly regulated during tumor metabolic reprogramming (Audrito et al., 2018). Moreover, expression of the other NBEs was only modestly affected by *FLVCR1a* knockdown (Figure S6C), with negligible effects on NAD^+ and NADH levels (Figure S6D). Accordingly, the NAD^+/NADH ratio was preserved (Figure S6E), indicating that *FLVCR1a* loss does not affect the levels of those coenzymes. The combined enhancement of both the TCA-cycle flux and OXPHOS probably accounts for the preserved NAD^+/NADH ratio observed in *FLVCR1a*-silenced cells.

Our data suggest that FLVCR1a controls the TCA cycle by modulating the intracellular heme pool involved in ALAS1 inhibition. Consistently, hemin administration in control Caco2 cells to induce feedback reduction of ALAS1 activity led to increased TCA-cycle flux, mimicking the effects of decreased heme export in *FLVCR1a*-silenced cells (Figure 3B). Moreover, we observed an increased TCA-cycle flux in *ALAS1*-silenced Caco2 cells (Figures 3C and S6F), similar to that reported for *FLVCR1a*-silenced cells. Conversely, *FLVCR1a*-overexpressing cells showed the opposite phenotype, with a significant reduction in the TCA-cycle flux, which could be reverted by treatment with hemin or with the heme synthesis inhibitor, SA (Figure 3D). Together, these findings strengthen the notion that FLVCR1a controls the TCA-cycle flux by modulating the rate of heme synthesis. The overall dataset indicates that FLVCR1a participates to the regulation of ALAS1 activity by modulating intracellular heme accumulation, with implications for the control of the TCA-cycle flux.

The heme synthesis-export system controls TCA-cycle fueling

The TCA cycle is a central hub for cell metabolic pathways. Metabolomic studies in Caco2 cells revealed a dramatic change in

Figure 3. The heme synthesis-export system controls the TCA cycle flux: Metabolic analyses at steady-state conditions

(A) *FLVCR1a*-silenced Caco2 cells are compared with cells expressing a scramble shRNA. TCA-cycle flux is reported in the center of the figure and is expressed as pmol CO_2/h/mg of protein. Data represent means ± SEM, n = 3. For statistical analyses, an unpaired Student's t test was used. $^{**}p < 0.01$. Moreover, TCA-cycle enzymes activities are reported in boxes and are expressed as mU/mg of mitochondrial proteins. Data represent means ± SEM, n = 3. For statistical analyses, an unpaired Student's t test was used. $^{*}p < 0.05$, $^{***}p < 0.001$. Finally, TCA cycle metabolite levels, except oxaloacetate, are shown and are expressed as μmol/g of proteins. Oxaloacetate levels are expressed as μmol/mg of proteins. Data represent mean ± SEM of n = 3 wells. For statistical analyses, an unpaired t test with Welch's correction was used for all the metabolites except oxaloacetate. $^{*}p < 0.05$. For oxaloacetate, an unpaired Student's t test was used. $^{**}p < 0.01$.

(B) TCA-cycle flux in Caco2 cells expressing a scramble shRNA untreated or treated with 25 μM of hemin for 2 h. Moreover, the TCA-cycle flux of untreated *FLVCR1a*-silenced Caco2 cells is reported for comparison. Results are expressed as pmol CO_2/h/mg of protein. Data represent means ± SEM, n = 3. For statistical analyses, an unpaired Student's t test was used to compare the two matched groups. $^{*}p < 0.05$, $^{***}p < 0.001$.

(C) TCA-cycle flux in Caco2 cells, in which the expression of *ALAS1* was downregulated using two specific shRNAs (*ALAS1* and *ALAS1*$_2$), compared with cells expressing a scramble shRNA. Results are expressed as pmol CO_2/h/mg of protein. Data represent means ± SEM, n = 3. For statistical analyses, an unpaired Student's t test was used. $^{*}p < 0.05$, $^{**}p < 0.01$.

(D) TCA-cycle flux in Caco2 cells overexpressing *FLVCR1a* (indicated as *FLVCR1a*$^+$) are compared with cells stably transduced with an empty vector. Moreover, the TCA-cycle flux of *FLVCR1a*-overexpressing Caco2 cells treated with 25 μM of hemin or 0.5 mM of SA for 2 h is reported. Results are expressed as pmol CO_2/h/mg of protein. Data represent means ± SEM, n = 3. For statistical analyses, an unpaired Student's t test was used to compare the two matched groups. $^{*}p < 0.05$, $^{**}p < 0.01$.

See also Figure S6.

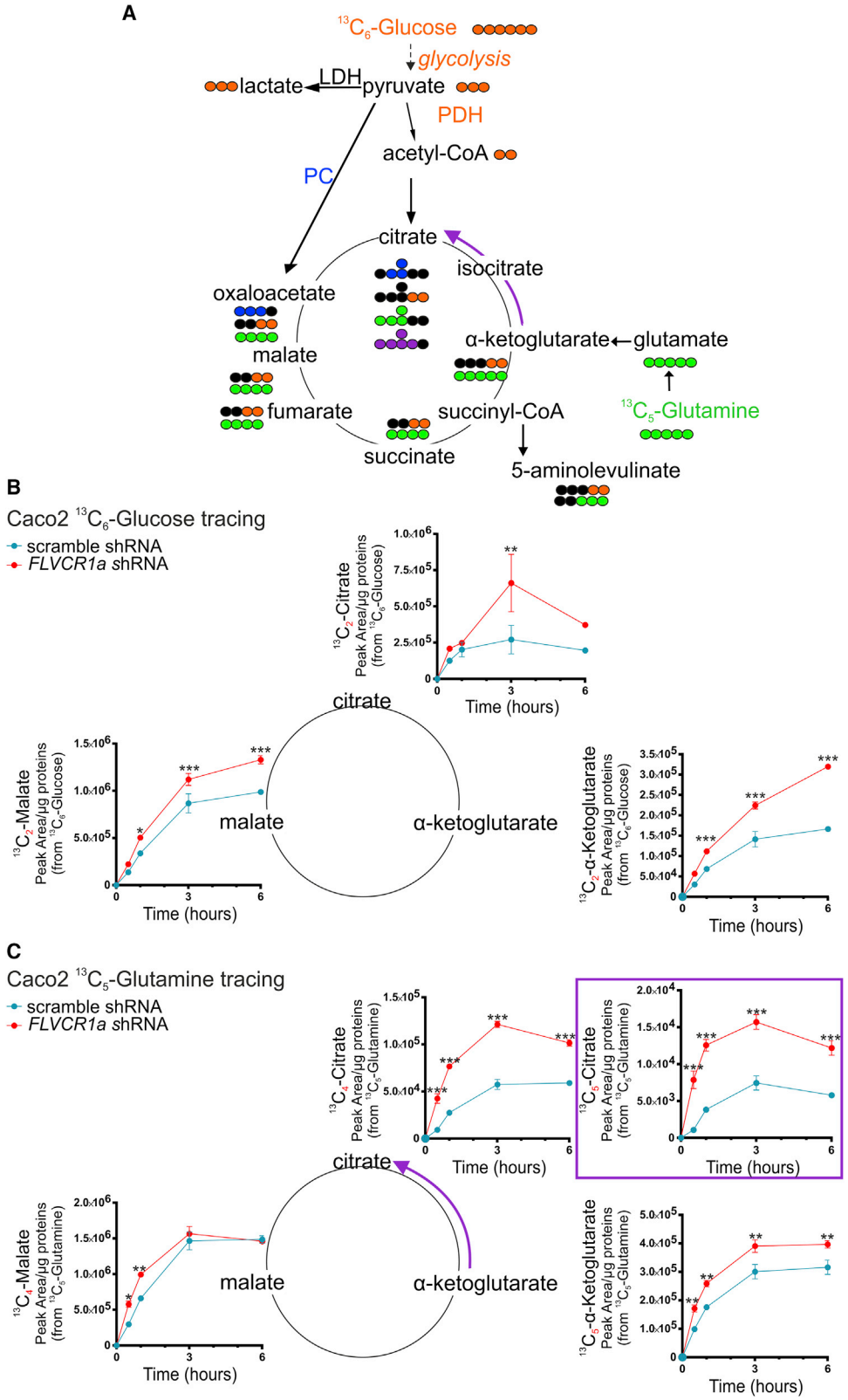

(legend on next page)

the profile of cell metabolites upon *FLVCR1a* silencing (Figure 5A), suggesting alterations in several metabolic reactions. Therefore, alterations in metabolites or metabolic pathways interlinked with the TCA cycle were explored.

Pyruvate levels were lower in *FLVCR1a*-silenced cells than they were in controls (Figure 5B), but that reduction could not be ascribed to defects in pyruvate production by the glycolytic pathway. Indeed, incorporation of labeled carbons in pyruvate from U-^{13}C-glucose was enhanced in *FLVCR1a*-silenced cells (Figure 5C), indicating increased glycolysis. Concomitantly, aerobic glycolysis was promoted, as demonstrated by high lactate production in *FLVCR1a*-silenced cells (Figure 5D). Furthermore, upon U-^{13}C-glucose administration, the amount of citrate $^{13}C_2$ and $^{13}C_3$ isotopologues (readouts of pyruvate dehydrogenase [PDH] and pyruvate carboxylase [PC] contribution to the TCA cycle, respectively) was higher in *FLVCR1a*-silenced cells than in controls (Figures 5E and 5F). These data indicate that, in addition to lactate dehydrogenase (LDH), both PDH and PC enzymes strongly consume pyruvate to sustain the TCA cycle in *FLVCR1a*-silenced cells and that TCA-cycle fueling by glucose is enhanced in *FLVCR1a*-silenced cells.

Additional pathways were then analyzed. Increased fatty acid β-oxidation was detected in *FLVCR1a*-silenced cells (Figure 5G). However, ketogenesis was also enhanced, as demonstrated by the higher amount of β-hydroxy-β-methylglutaryl-CoA (HMG-CoA) and β-hydroxybutyrate (β-OH-butyrate) (Figure 5H). Because ketogenesis consumes the acetyl-CoA produced by fatty acids β-oxidation, the data suggest that the surplus of fatty acid β-oxidation detected in *FLVCR1a*-silenced cells provides a poor contribution to TCA-cycle fueling. Conversely, tracing analyses of *FLVCR1a*-silenced cells with U-^{13}C-glutamine showed enhanced incorporation of labeled carbons in glutamate (Figure 6A) and, as stated previously, in α-ketoglutarate (Figure 4C), indicating increased glutaminolysis. That conclusion was supported by the detection of greater glutaminase (GLS) and less glutamine synthetase (GLUL) activity in *FLVCR1a*-silenced Caco2 cells than found in controls (Figure 6B). These results, together with those illustrating enhanced oxidation/reductive carboxylation of glutamine, attest to increased TCA-cycle fueling by glutamine in *FLVCR1a*-silenced cells.

Finally, when compared with controls, *FLVCR1a*-silenced cells showed reduced total γ-aminobutyric acid (GABA) levels (Figure 6C) and increased incorporation of labeled carbons from U-^{13}C-glucose or U-^{13}C-glutamine into succinate semialdehyde (SSA) (Figures 6D and 6E), an intermediate produced when GABA is converted by GABA transaminase into succinate through the GABA shunt. Together, these results indicate increased TCA-cycle anaplerosis by GABA.

Overall, reduced heme synthesis-export results in the promotion of the TCA cycle and in the recruitment of several pathways to sustain it, with consequences on the rate of OXPHOS.

Relevance of the heme synthesis-export system *in vivo*

Mining of the BioXpress database (Wan et al., 2015) revealed overexpression of *FLVCR1* in several tumor types other than CRC (Figure 7A), suggesting that the ALAS1-FLVCR1a system could be exploited to modulate oxidative metabolism in different tumor contexts. To address that point, we down-modulated *FLVCR1a* in neuroblastoma SH-SY5Y cells (Figures S7A and S7B) and in tumor endothelial cells (BTECs, breast-cancer-derived tumor endothelial cells) (Figures S7C and S7D). We chose such models based on previous observations that FLVCR1 inactivation leads to reduced survival/proliferation in the nervous and endothelial system (Chiabrando et al., 2016; Petrillo et al., 2018; Bertino et al., 2019).

In SH-SY5Y cells, *FLVCR1a* silencing resulted in greater heme accumulation than controls upon stimulation of *de novo* heme biosynthesis (Figure S7E); in BTECs, increased heme levels were already detectable at the steady state after *FLVCR1a* knockdown (Figure S7F), indicating that, in these cell lines, *FLVCR1a* down-modulation also blocks heme efflux. Moreover, in both *FLVCR1a*-silenced cell lines, we observed enhanced activity of ETC complexes with increased mitochondrial ATP levels (Figures 7B, 7C, S7G, and S7H) as well as increased TCA-cycle flux (Figures 7D and S7I), confirming the observations obtained in the CRC cell lines.

Finally, to evaluate the *in vivo* relevance of our findings, we took advantage of tamoxifen-inducible endothelial-specific *Flvcr1a*-null mice (*Flvcr1a*$^{fl/fl}$;Cdh5(PAC)-Cre^{ERT2}) (Figure 7E) and analyzed oxidative metabolism in tumor endothelial cells (TECs) isolated from subcutaneous tumors. As observed *in vitro* and in *Flvcr1a*-deleted endothelial cells (indicated as *Flvcr1a*-KO), the activity of TCA-cycle enzymes (Figure 7F) and that of ETC complexes and the levels of mitochondrial ATP (Figures 7G and 7H) were higher than in control counterparts. These data support the notion that FLVCR1a-mediated heme export modulates TCA cycle and OXPHOS.

Figure 4. The heme synthesis-export system controls the TCA cycle flux: Time-course metabolic analyses, with *FLVCR1a*-silenced Caco2 cells compared with cells expressing a scramble shRNA

(A) Predicted labeling pattern of the indicated metabolites in cells cultured with U-^{13}C-glucose or U-^{13}C-glutamine. Colored and black circles indicate ^{13}C and ^{12}C carbon units, respectively. Orange circles indicate ^{13}C carbon units derived from U-^{13}C-glucose. When pyruvate carboxylase (PC) catalyzes the reaction, the ^{13}C carbon units derived from U-^{13}C-glucose are depicted in blue. Green circles indicate ^{13}C carbon units derived from U-^{13}C-glutamine. When reductive carboxylation occurs, the ^{13}C carbon units derived from U-^{13}C-glutamine are represented in violet. PDH, pyruvate dehydrogenase; LDH, lactate dehydrogenase.
(B) Accumulation of $^{13}C_2$-citrate, $^{13}C_2$-α-ketoglutarate, and $^{13}C_2$-malate in cells incubated with U-^{13}C-glucose for the indicated time. Data represent means ± SEM, n = 4 wells pooled from two independent experiments. For statistical analyses, a two-way analysis of variance was used, followed by the Bonferroni correction for multiple group comparisons. *p < 0.05, **p < 0.01, ***p < 0.001.
(C) Accumulation of $^{13}C_4$-citrate, $^{13}C_5$-α-ketoglutarate and $^{13}C_4$-malate in cells incubated with U-^{13}C-glutamine for the indicated time. Accumulation of $^{13}C_5$-citrate derived from reductive carboxylation (violet arrow) is reported in the violet box. Data represent means ± SEM, n = 4 wells pooled from two independent experiments. For statistical analyses, a two-way analysis of variance was used, followed by the Bonferroni correction for multiple group comparisons. *p < 0.05, **p < 0.01, ***p < 0.001.

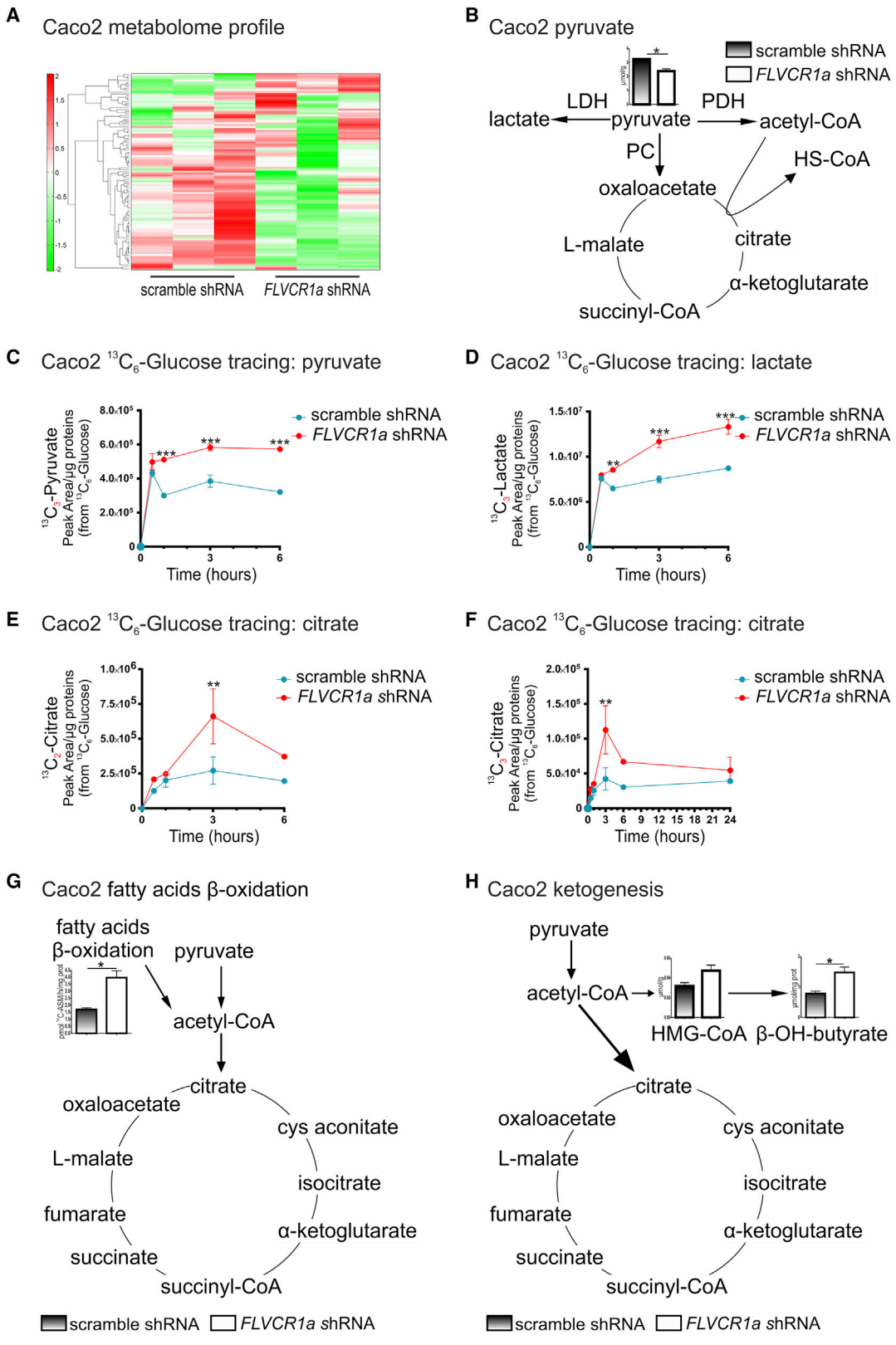

(legend on next page)

DISCUSSION

The results described here illustrate the functionality of a heme synthesis-export axis adopted by cells to reduce the TCA-cycle flux and its fueling with the ensuing reduction of OXPHOS.

Previous work from our laboratory has demonstrated that there is a strong relationship between heme synthesis and heme export, whereby the pool of newly synthetized heme is controlled by the concerted actions of the heme synthetic enzyme ALAS1 and the heme exporter FLVCR1a. For example, in hepatic cells from liver-specific *Flvcr1a*-null mice, reduced ALAS1 activity was detected (Vinchi et al., 2014). Moreover, liver cells from wild-type mice displayed co-regulation of *Alas1* and *Flvcr1* gene expression in response to 5-ALA (Vinchi et al., 2014). Similarly, *FLVCR1b*-overexpressing HeLa cells exhibited more mRNA for several heme biosynthetic enzymes and an increased heme content, which could be prevented by treatment with the heme synthesis inhibitor SA (Chiabrando et al., 2012), indicating increased heme synthesis when heme export is enhanced. Data presented in this work confirm the relationship between heme production and export and provide evidence that the heme synthesis-export system critically contributes to TCA-cycle flux and OXPHOS.

Results from several studies have documented that ALAS1, the rate limiting enzyme of the heme biosynthetic pathway, is negatively regulated by heme itself (Zheng et al., 2008; Kubota et al., 2016; Srivastava et al., 1988; Lathrop and Timko, 1993). Heme controls transcription (Yamamoto et al., 1982), translation (Sassa and Granick, 1970; Yamamoto et al., 1983), and stability (Hamilton et al., 1991) of *ALAS1* mRNA. Moreover, heme binding to heme regulatory motifs, situated in the mitochondrial targeting sequence of ALAS1, inhibits protein translocation to the mitochondria (Yamauchi et al., 1980). We found that FLVCR1a-mediated heme export introduces a further level of regulation by controlling the size of the regulatory heme pool responsible for ALAS1 modulation.

The observed enhancement of heme synthesis associated with reduced activity of ETC complexes, which exploit heme as a co-factor, is counterintuitive. Moreover, our data are in apparent contrast to other studies showing that the administration of exogenous heme promotes ETC activity (Vandekeere et al., 2018). Our finding that the administration of exogenous heme phenocopied *FLVCR1a* and *ALAS1* silencing, leading to increased TCA-cycle flux, which, in turn, supports the activity of ETC complexes, provides an alternative explanation for such seemingly discrepant observations. Moreover, when comparing the effects of *FLVCR1a* silencing versus *ALAS1* silencing on the activity of ETC complexes, the *FLVCR1a*-controlled heme pool appears to regulate cellular respiration indirectly through the TCA cycle and not directly by regulating heme supply to ETC complexes.

The modulation of the TCA cycle by the heme synthesis-export axis might be explained by ALAS1-mediated TCA-cycle cataplerosis, a process whose importance is also supported by literature data: experimental models of hereditary leiomyomatosis and renal-cell cancer, which bear inactivating mutation in fumarate hydratase, show increased heme synthesis and dependence on the heme-degrading enzyme HMOX-1 for survival (Frezza et al., 2011).

In addition to cataplerosis, other heme-controlled events may contribute to the modulation of the TCA cycle. We found that TCA-cycle fueling, by both glucose and glutamine, is enhanced when the heme synthesis-export axis is inhibited. This is in agreement with data showing heme-dependent control of PDH, a key enzyme for supply of the TCA cycle by glucose (Lynch et al., 2019) and with the observation that the heme-regulated transcription factor BTB and CNC homology 1 (BACH1) modulates the expression of the glycolytic enzymes hexokinase 2 and glyceraldehyde-3-phosphate dehydrogenase (GAPDH) (Wiel et al., 2019) and the activity of PDH (Lee et al., 2019).

Altogether, these data suggest that heme efflux by FLVCR1a finely tunes the rate of heme synthesis required for TCA-cycle cataplerosis and for the establishment of a regulatory heme pool that participates in the transcriptional regulation of genes involved in TCA fueling. The induction of the heme synthesis-export system represents a strategy adopted by cells to shut down oxidative metabolism and ensure adequate heme supply for hemoproteins' production.

Metabolic alterations promoted by *FLVCR1a* silencing in CRC cell lines were associated with reduced proliferation and increased apoptosis. Similarly, *FLVCR1a* down-modulation in synovial sarcoma cells (Peng et al., 2018) and in other transformed cell lines (Chiabrando et al., 2016; Mercurio et al., 2015) led to impaired proliferation/survival. Moreover, *FLVCR1a* is overexpressed in several cancer types, and accumulating evidence points to an essential role for heme synthesis in cancer (Fiorito et al., 2020). Increased heme synthesis in tumors versus healthy tissues is exploited for tumor fluorescence-guided surgery (FGS) and to kill cancer cells by photodynamic therapy (PDT) (Malik and Lugaci, 1987; Kennedy et al., 1990; Peng

Figure 5. The heme synthesis-export system controls the TCA-cycle fueling: Glucose and fatty acids, with *FLVCR1a*-silenced Caco2 cells compared with cells expressing a scramble shRNA

(A) Heatmap representation of metabolome profiles analyzed by hierarchical clustering analysis, n = 3 wells.

(B) Pyruvate levels. Values are expressed as μmol/g of proteins. Data represent means ± SEM of n = 3 wells. For statistical analyses, an unpaired t test with Welch's correction was used. *p < 0.05.

(C–F) Accumulation of $^{13}C_3$-pyruvate (C), $^{13}C_3$-lactate (D), $^{13}C_2$-citrate (E), and $^{13}C_3$-citrate (F) in cells incubated with U-^{13}C-glucose for the indicated time. Data represent means ± SEM, n = 4 wells pooled from two independent experiments. For statistical analyses, a two-way analysis of variance was used, followed by the Bonferroni correction for multiple group comparisons. **p < 0.01, ***p < 0.001.

(G) Fatty acids β-oxidation. Values are expressed as pmol of ^{14}C-acid soluble metabolites (^{14}C-ASM)/h/mg of proteins. Data represent means ± SEM of n = 3 wells. For statistical analyses, an unpaired Student's t test was used. *p < 0.05.

(H) β-hydroxy-β-methylglutaryl-CoA (HMG-CoA) and β-hydroxybutyrate (β-OH-butyrate) levels expressed as μmoles/mg of cellular proteins and μmoles/g of cellular proteins, respectively. The measure of the two metabolites was considered as an index of ketone bodies amount. Data represent means ± SEM, n = 3. For statistical analyses, for HMG-CoA an unpaired t test with Welch's correction was used, and for β-OH-butyrate, an unpaired Student's t test was used. *p < 0.05.

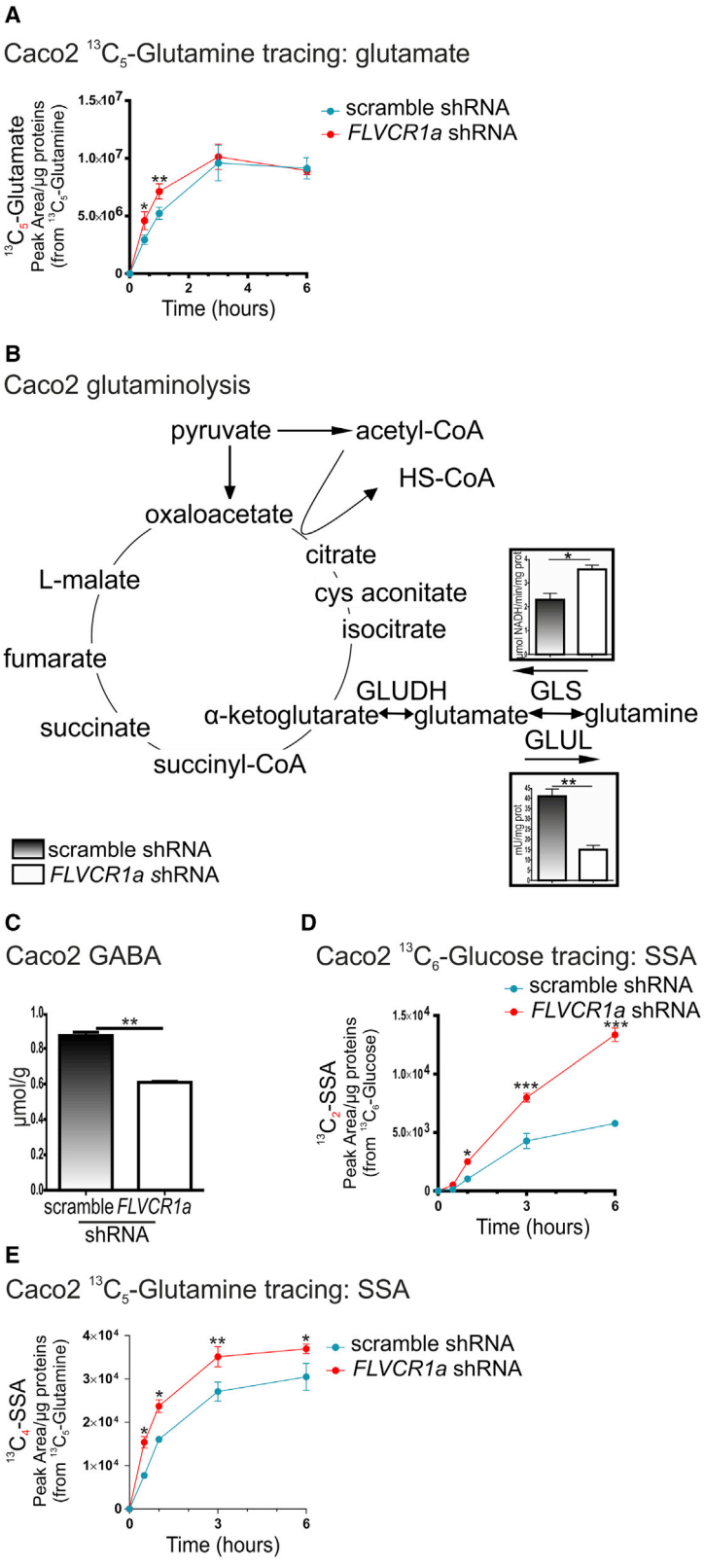

Figure 6. The heme synthesis-export system controls the TCA cycle fueling: Glutamine and GABA, with *FLVCR1a*-silenced Caco2 cells compared with cells expressing a scramble shRNA

(A) Accumulation of $^{13}C_5$-glutamate in cells incubated with U-^{13}C-glutamine for the indicated time. Values are expressed as peak area/µg of proteins. Data represent means ± SEM of n = 4 wells pooled from two independent experiments. For statistical analyses, a two-way analysis of variance was used, followed by the Bonferroni correction for multiple group comparisons. *p < 0.05, **p < 0.01.

(B) Glutaminase (GLS) and glutamine synthetase (GLUL) activities are reported in gray background boxes and are expressed as µmol of NADH/min/mg cellular proteins or mU/mg of cellular proteins, respectively. Data represent means ± SEM, n = 3. For statistical analyses, an unpaired Student's t test was used. *p < 0.05, **p < 0.01.

(C) γ-aminobutyric acid (GABA) levels expressed as µmol/g of proteins. Data represent means ± SEM of n = 3 wells. For statistical analyses, an unpaired t test with Welch's correction was used. **p < 0.01.

(D and E) Accumulation of $^{13}C_2$-succinate semialdehyde ($^{13}C_2$-SSA) in cells incubated with U-^{13}C-glucose (D) or of $^{13}C_4$-SSA in cells incubated with U-^{13}C-glutamine (E) for the indicated time. Values are expressed as peak area/µg of proteins. Data represent means ± SEM of n = 4 wells pooled from two independent experiments. For statistical analyses, a two-way analysis of variance was used, followed by the Bonferroni correction for multiple group comparisons. *p < 0.05, **p < 0.01, ***p < 0.001.

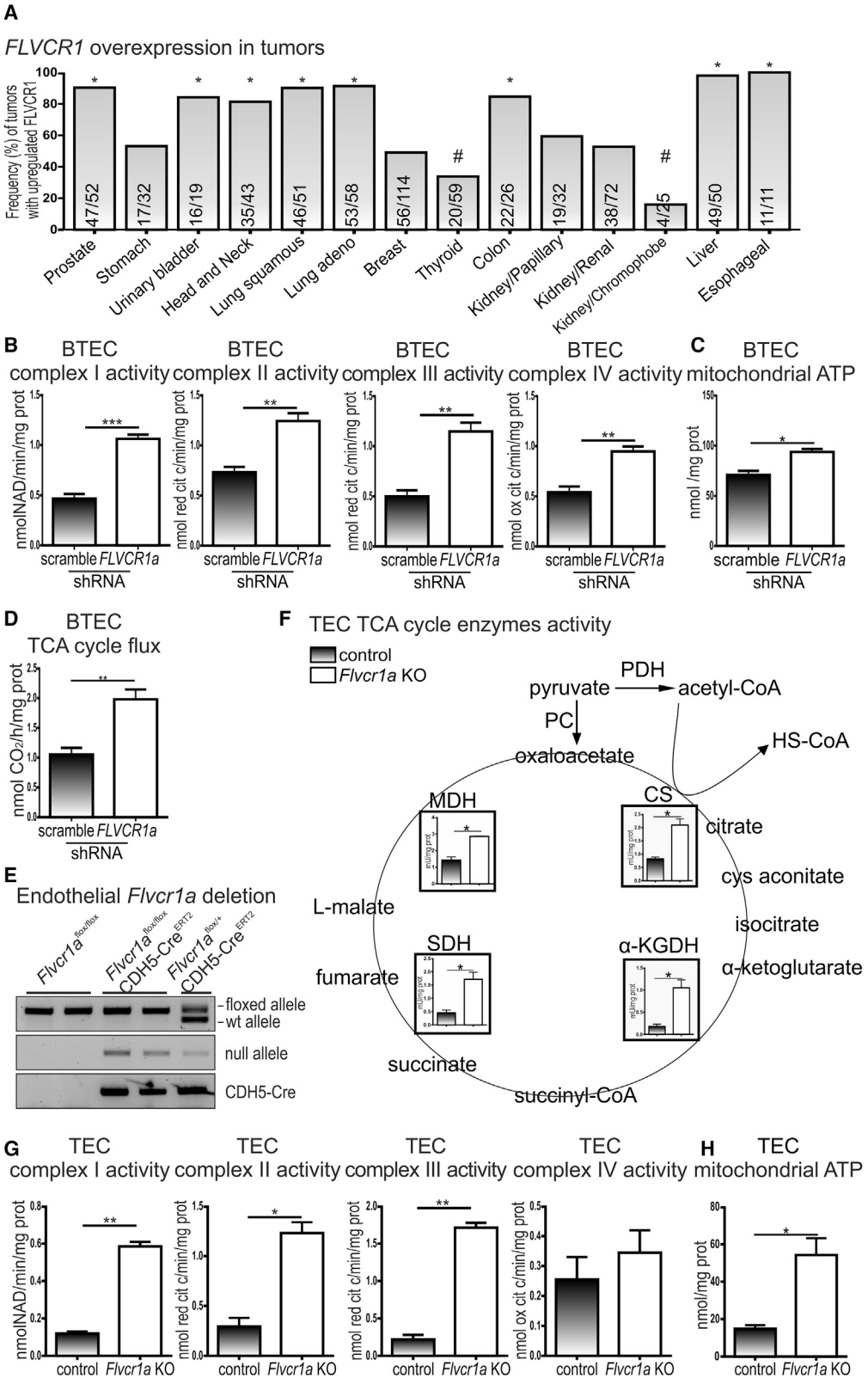

(legend on next page)

et al., 1992). The growth-inhibitory effects of *FLVCR1* knockdown could be ascribed to its effect on the heme synthesis-export axis, leading to the forced implementation of oxidative metabolism and the compensatory engagement of several pathways to sustain the TCA cycle. Several other factors might also contribute to reduced cell viability after *FLVCR1a* inactivation. Heme synthesis is required to sustain the expression/activity of several hemoproteins crucial for survival and proliferation, including cyclooxygenases, catalases, peroxidases among others (Chiabrando et al., 2014); in addition, dysregulated heme metabolism promotes oxidative stress responsible for DNA, lipid, and protein damage (Chiabrando et al., 2014).

We show here that *Flvcr1a* loss in endothelial cells *in vivo* results in enhanced TCA-cycle flux and OXPHOS, similar to that reported for cultured endothelial cells and cancer cell lines. Because endothelial cells mainly rely on aerobic glycolysis for energy supply, these data indicate that they depend on the heme synthesis-export axis to repress oxidative metabolism. Moreover, *FLVCR1a* silencing in endothelial cells reduces proliferation/survival, in line with previous findings documenting abnormal vascular development and embryo lethality in mice with constitutive *Flvcr1a* loss in the endothelium (Petrillo et al., 2018). We can, therefore, speculate that the metabolic adaptation modulated by the heme synthesis-export axis contributes to sustaining proliferation/survival, not only in tumor cells but also in endothelial cells. A crucial role for FLVCR1a in proliferating cells is also supported by the observation that mice with intestine-specific *Flvcr1a* knockout display reduced proliferation of intestinal mucosa cells in physiological conditions and reduced survival upon experimental induction of ulcerative colitis, a pathological state requiring regeneration of the intestinal mucosa (Fiorito et al., 2015). Moreover, the role of FLVCR1 in the maturation of erythroid progenitors and in embryo development has been extensively documented (Keel et al., 2008; Petrillo et al., 2018; Doty et al., 2015; Mercurio et al., 2015). Altogether, these data suggest that the metabolic rewiring regulated by the heme synthesis-export system supports cell proliferation.

Heme synthesis is a constitutive process regulated at several levels. Data in mice indicate that all cells need to export heme through FLVCR1a, as evidenced by the embryonic lethal phenotype of animals with constitutive *Flvcr1a* loss and organ abnormalities in conditional models. This conclusion is also supported by data in humans indicating that *FLVCR1* gene mutations associated to specific disorders do not completely abrogate the heme efflux function, which attests to the hypomorphic nature of such mutations. Thus, we can speculate that the heme synthesis-export system represents a physiological mechanism to maintain heme homeostasis. Interestingly, *FLVCR1* is induced by hypoxia, strengthening the concept that the ALAS1-FLVCR1a axis is required to shut down oxidative metabolism, an absolute requirement when oxygen availability is limiting. Further studies are required to better define the role of the heme synthesis-export system in physiologic and pathologic conditions.

The TCA cycle is a central hub for cell energy metabolism, the synthesis of macromolecules, and redox balance. Impaired TCA-cycle functions are associated with a wide variety of

Figure 7. Relevance of the heme synthesis-export system *in vivo*

(A) Frequency (%) of patient tumors with overexpression of *FLVCR1* compared with their matched normal tissues across multiple cancer types. The number of patients showing tumor *FLVCR1* overexpression relative to the total number of patients examined is indicated in the plot. Data derive from BioXpress (Wan et al., 2015). For statistical analyses, a binomial test was used, with the null hypothesis being equal probability of *FLVCR1* being up or downregulated in cancer for each patient. $p < 0.01$ was regarded as significant; *$p < 0.01$ (in all significant cases in which the number of patients with *FLVCR1* overexpression is significantly greater than expected in the null hypothesis). #$p < 0.01$ (in all significant cases in which the number of patients with *FLVCR1* overexpression is significantly less than expected in the null hypothesis).

(B) Activities of the mitochondrial electron transport chain complexes I–IV in *FLVCR1a*-silenced BTECs compared with cells expressing a scramble shRNA. Results were expressed as nmol NAD^+/min/mg of mitochondrial protein for complex I, nmol reduced cytochrome *c*/min/mg of mitochondrial protein for complexes II–III, AND nmol oxidized cytochrome *c*/min/mg of mitochondrial protein for complex IV. Data represent means ± SEM, n = 3. For statistical analyses, an unpaired Student's t test was used. **$p < 0.01$, *$p < 0.001$.

(C) Mitochondrial ATP levels measured by a bioluminescent assay kit in *FLVCR1a*-silenced BTECs compared with cells expressing a scramble shRNA. Results are expressed as nmol/mg of mitochondrial proteins. Data represent means ± SEM, n = 3. For statistical analyses, an unpaired Student's t test was used. *$p < 0.05$.

(D) TCA-cycle flux in *FLVCR1a*-silenced BTECs compared with cells expressing a scramble shRNA. Results are expressed as pmol CO_2/h/mg of protein. Data represent means ± SEM, n = 3. For statistical analyses, an unpaired Student's t test was used. **$p < 0.01$.

(E) Polymerase chain reaction (PCR) on *Flvcr1a*$^{fl/fl}$;Cdh5(PAC)-Cre^{ERT2} mice and control *Flvcr1a*$^{fl/fl}$ mice after tamoxifen injection. Specific primers allowed the distinction of the wild-type (242 bp), floxed (280 bp), and null allele (320 bp) of *Flvcr1a*. Deletion of the first exon of *Flvcr1a* gene mediated by CRE recombinase gives rise to a band referred to as the "null allele."

(F) TCA-cycle enzymes activities are reported in boxes and expressed as mU/mg of mitochondrial proteins. Tumor endothelial cells (TECs) isolated by subcutaneous tumors in tamoxifen-inducible endothelial specific *Flvcr1a* null mice (*Flvcr1a*$^{fl/fl}$;Cdh5(PAC)-Cre^{ERT2} indicated as *Flvcr1a*-KO) are compared with TECs isolated by subcutaneous tumors in control *Flvcr1a*$^{fl/fl}$ mice. Data represent means ± SEM, n = 2 pools of animals. For statistical analyses, an unpaired Student's t test was used. *$p < 0.05$.

(G) Activities of the mitochondrial electron transport chain complexes I–IV in TECs isolated by subcutaneous tumors in tamoxifen-inducible endothelial specific *Flvcr1a*-null mice (*Flvcr1a*$^{fl/fl}$;Cdh5(PAC)-Cre^{ERT2} indicated as *Flvcr1a*-KO) are compared with TECs isolated by subcutaneous tumors in control *Flvcr1a*$^{fl/fl}$ mice. Results were expressed as nmol NAD^+/min/mg of mitochondrial protein for complex I, nmol reduced cytochrome *c*/min/mg of mitochondrial protein for complexes II–III, and nmol oxidized cytochrome *c*/min/mg of mitochondrial protein for complex IV. Data represent means ± SEM, n = 2 pools of animals. For statistical analyses, an unpaired Student's t test was used. *$p < 0.05$, **$p < 0.01$.

(H) Mitochondrial ATP levels measured with a bioluminescent assay kit in TECs isolated by subcutaneous tumors in tamoxifen-inducible endothelial-specific *Flvcr1a*-null mice (*Flvcr1a*$^{fl/fl}$;Cdh5(PAC)-Cre^{ERT2} indicated as *Flvcr1a*-KO) are compared with TECs isolated by subcutaneous tumors in control *Flvcr1a*$^{fl/fl}$ mice. Results are expressed as nmol/mg of mitochondrial proteins. Data represent means ± SEM, n = 2 pools of animals. For statistical analyses, an unpaired Student's t test was used. *$p < 0.05$.

See also Figure S7.

pathological processes, encompassing cancer, obesity, neurodegenerative disorders, infections, muscular diseases, and diabetes among others. Several components or indirect modulators of the TCA cycle may be exploited for therapeutic purposes and, although high toxicity remains an issue, some of those approaches have proven to be well tolerated clinically (Anderson et al., 2018). Our data identified the heme synthesis-export axis as a potentially targetable vulnerability to modulate the TCA-cycle flux. The fact that FLVCR1a is a plasma membrane protein makes it a good candidate for the development of specific inhibitors/activators, particularly in the context of cancer, in which this heme exporter is overexpressed compared with that of normal tissues. Moreover, some U.S. Food and Drug Administration (FDA)-approved drugs expected to inhibit/enhance heme synthesis and heme export are already available (Wachowska et al., 2011; Webber et al., 1999; Stein et al., 2017) and could be used to interfere with cell metabolic adaptation in various disease types. In conclusion, our work identifies the heme synthesis-export axis as a key regulator of the TCA cycle and oxidative metabolism and puts forth the potential targeting of this system in various pathological settings.

STAR★METHODS

Detailed methods are provided in the online version of this paper and include the following:

- KEY RESOURCES TABLE
- RESOURCE AVAILABILITY
  - Lead contact
  - Materials availability
  - Data and code availability
- EXPERIMENTAL MODEL AND SUBJECT DETAILS
  - Cell lines
  - Animal models
- METHOD DETAILS
  - Analyses on human samples databases
  - Gene silencing and overexpression
  - Tumor-associated endothelial cells isolation
  - Xenograft tumor model
  - Hematoxylin and eosin staining
  - Cell viability assay
  - Crystal Violet staining
  - Apoptosis analysis
  - Hemin, 5-ALA and SA cell treatment
  - RNA extraction and quantitative real-time PCR analysis
  - Western blot analysis
  - Zinc-mesoporphyrin washout experiments
  - Measurement of heme concentration
  - Metabolome analysis
  - Assessment of metabolites levels
  - NAD+ and NADH levels assessment
  - ^{13}C-isotope labeling experiments
  - Mitochondria isolation
  - Citrate synthase, α-ketoglutarate dehydrogenase, succinate dehydrogenase and malate dehydrogenase activities
  - Activity of mitochondrial ETC complexes I-IV
  - Oxygen consumption rate measurement
  - Measurement of total cellular ATP levels
  - Measurements of cytosolic ATP levels
  - ATP levels in mitochondria and activity of mitochondrial ATP-synthase
  - Adenine nucleotide translocases (ANTs) activity
  - Tricarboxylic acid (TCA) cycle flux
  - Glutaminase (GLS) and glutamine synthetase (GLUL) activity
  - Fatty acids β-oxidation measurement
  - Ketone bodies measurement
  - Mitochondrial biogenesis
  - Mitochondrial basal calcium levels measurement
  - Mitochondrial calcium uptake measurement
  - Mitochondrial membrane potential measurements
- QUANTIFICATION AND STATISTICAL ANALYSIS

SUPPLEMENTAL INFORMATION

Supplemental information can be found online at https://doi.org/10.1016/j.celrep.2021.109252.

ACKNOWLEDGMENTS

The authors are grateful to Drs. Francesco Sassi and Marco Forni for help with histological analyses, to Prof. Benedetta Bussolati for providing BTECs, to Dr. Lucia Lecce for oxygen consumption rate analyses, and to Prof. Claudia Piccoli for helpful discussion. This work was supported by the Italian Association for Cancer Research (AIRC) grants IG18857 and IG24922 to E.T., IG22802 to L.T., IG21408 to C.R., and IG21923 to A.B.; AIRC Start-Up 2017 ID 20464 to S.C.; AIRC 5x1000 grant 21091 to L.T. and A.B.; AIRC/CRUK/FC AECC Accelerator Award 22795 to L.T. and A.B.; Fondazione Cassa di Risparmio di Torino grant 2018/2260 to E.T.; and the Italian Regenerative Medicine Infrastructure (IRMI) grant CTN01_00177_888744 to F.A.

AUTHOR CONTRIBUTIONS

Conceptualization, V.F. and E.T.; methodology, V.F., S.P., and E.T.; formal analysis, V.F., S.M., P. Provero, and S.C.; investigation, V.F., A.L.A., S.P., E.G., S.T., S.M., S.C., F.D., C.P., V.A., and P. Provero; resources, E.T., S.C., P. Provero, E.M., C.C., A.B., S.D., F.A., C.R., and P. Pinton; writing – original draft, V.F. and E.T.; writing – review & editing, V.F., E.T., A.L.A., S.P., S.M., F.D., S.C., V.A., P. Provero, E.M., D.C., P.E.P., A.B., L.T., N.C., S.D., F.A., C.R., and P. Pinton; visualization, V.F. and E.T.; supervision, E.T.; project administration, E.T. and V.F.; funding acquisition: E.T., C.R., L.T., S.C., A.B., and F.A.

DECLARATION OF INTERESTS

A.B. is a founder and a shareholder of Neophore; is an advisory board member for Roche, Inivata, Neophore, and Phoremost; has received grant support from AstraZeneca. L.T. receives research grants from Symphogen, Servier, Pfizer, Menarini, Merck KGaA, and Merus; and is in the speakers' bureau of Eli Lilly, AstraZeneca, and Merck KGaA. E.T., V.F., A.L.A, S.P., and D.C. hold a pending patent application related to this work. The other authors declare no competing interests.

Received: April 17, 2020
Revised: December 21, 2020
Accepted: May 25, 2021
Published: June 15, 2021

REFERENCES

Anderson, N.M., Mucka, P., Kern, J.G., and Feng, H. (2018). The emerging role and targetability of the TCA cycle in cancer metabolism. Protein Cell *9*, 216–237.

Audrito, V., Managò, A., La Vecchia, S., Zamporlini, F., Vitale, N., Baroni, G., Cignetto, S., Serra, S., Bologna, C., Stingi, A., et al. (2018). Nicotinamide phosphoribosyltransferase (NAMPT) as a therapeutic target in BRAF-mutated metastatic melanoma. J. Natl. Cancer Inst. *110*, 290–303.

Azuma, M., Kabe, Y., Kuramori, C., Kondo, M., Yamaguchi, Y., and Handa, H. (2008). Adenine nucleotide translocator transports haem precursors into mitochondria. PLoS ONE *3*, e3070.

Barupala, D.P., Dzul, S.P., Riggs-Gelasco, P.J., and Stemmler, T.L. (2016). Synthesis, delivery and regulation of eukaryotic heme and Fe-S cluster cofactors. Arch. Biochem. Biophys. *592*, 60–75.

Bertino, F., Firestone, K., Bellacchio, E., Jackson, K.E., Asamoah, A., Hersh, J., Fiorito, V., Destefanis, F., Gonser, R., Tucker, M.E., et al. (2019). Heme and sensory neuropathy: insights from novel mutations in the heme exporter feline leukemia virus subgroup C receptor 1. Pain *160*, 2766–2775.

Bonora, M., Giorgi, C., Bononi, A., Marchi, S., Patergnani, S., Rimessi, A., Rizzuto, R., and Pinton, P. (2013). Subcellular calcium measurements in mammalian cells using jellyfish photoprotein aequorin-based probes. Nat. Protoc. *8*, 2105–2118.

Capello, M., Ferri-Borgogno, S., Riganti, C., Chattaragada, M.S., Principe, M., Roux, C., Zhou, W., Petricoin, E.F., Cappello, P., and Novelli, F. (2016). Targeting the Warburg effect in cancer cells through ENO1 knockdown rescues oxidative phosphorylation and induces growth arrest. Oncotarget *7*, 5598–5612.

Chiabrando, D., Marro, S., Mercurio, S., Giorgi, C., Petrillo, S., Vinchi, F., Fiorito, V., Fagoonee, S., Camporeale, A., Turco, E., et al. (2012). The mitochondrial heme exporter FLVCR1b mediates erythroid differentiation. J. Clin. Invest. *122*, 4569–4579.

Chiabrando, D., Vinchi, F., Fiorito, V., Mercurio, S., and Tolosano, E. (2014). Heme in pathophysiology: a matter of scavenging, metabolism and trafficking across cell membranes. Front. Pharmacol. *5*, 61.

Chiabrando, D., Castori, M., di Rocco, M., Ungelenk, M., Gießelmann, S., Di Capua, M., Madeo, A., Grammatico, P., Bartsch, S., Hübner, C.A., et al. (2016). Mutations in the heme exporter FLVCR1 cause sensory neurodegeneration with loss of pain perception. PLoS Genet. *12*, e1006461.

Curthoys, N.P., and Weiss, R.F. (1974). Regulation of renal ammoniagenesis: subcellular localization of rat kidney glutaminase isoenzymes. J. Biol. Chem. *249*, 3261–3266.

Destefanis, F., Fiorito, V., Altruda, F., and Tolosano, E. (2019). Investigating the connection between endogenous heme accumulation and COX2 activity in cancer cells. Front. Oncol. *9*, 162.

Doty, R.T., Phelps, S.R., Shadle, C., Sanchez-Bonilla, M., Keel, S.B., and Abkowitz, J.L. (2015). Coordinate expression of heme and globin is essential for effective erythropoiesis. J. Clin. Invest. *125*, 4681–4691.

Fiorito, V., Forni, M., Silengo, L., Altruda, F., and Tolosano, E. (2015). Crucial role of FLVCR1a in the maintenance of intestinal heme homeostasis. Antioxid. Redox Signal. *23*, 1410–1423.

Fiorito, V., Chiabrando, D., Petrillo, S., Bertino, F., and Tolosano, E. (2020). The multifaceted role of heme in cancer. Front. Oncol. *9*, 1540.

Frezza, C., Zheng, L., Folger, O., Rajagopalan, K.N., MacKenzie, E.D., Jerby, L., Micaroni, M., Chaneton, B., Adam, J., Hedley, A., et al. (2011). Haem oxygenase is synthetically lethal with the tumour suppressor fumarate hydratase. Nature *477*, 225–228.

Fukuda, Y., Wang, Y., Lian, S., Lynch, J., Nagai, S., Fanshawe, B., Kandilci, A., Janke, L.J., Neale, G., Fan, Y., et al. (2017). Upregulated heme biosynthesis, an exploitable vulnerability in MYCN-driven leukemogenesis. JCI Insight *2*, e92409.

Gaster, M., Rustan, A.C., Aas, V., and Beck-Nielsen, H. (2004). Reduced lipid oxidation in skeletal muscle from type 2 diabetic subjects may be of genetic origin: evidence from cultured myotubes. Diabetes *53*, 542–548.

Giraud, S., Bonod-Bidaud, C., Wesolowski-Louvel, M., and Stepien, G. (1998). Expression of human ANT2 gene in highly proliferative cells: GRBOX, a new transcriptional element, is involved in the regulation of glycolytic ATP import into mitochondria. J. Mol. Biol. *281*, 409–418.

Gotoh, T., Terada, K., Oyadomari, S., and Mori, M. (2004). hsp70-DnaJ chaperone pair prevents nitric oxide- and CHOP-induced apoptosis by inhibiting translocation of Bax to mitochondria. Cell Death Differ. *11*, 390–402.

Grange, C., Bussolati, B., Bruno, S., Fonsato, V., Sapino, A., and Camussi, G. (2006). Isolation and characterization of human breast tumor-derived endothelial cells. Oncol. Rep. *15*, 381–386.

Hamilton, J.W., Bement, W.J., Sinclair, P.R., Sinclair, J.F., Alcedo, J.A., and Wetterhahn, K.E. (1991). Heme regulates hepatic 5-aminolevulinate synthase mRNA expression by decreasing mRNA half-life and not by altering its rate of transcription. Arch. Biochem. Biophys. *289*, 387–392.

Jouaville, L.S., Pinton, P., Bastianutto, C., Rutter, G.A., and Rizzuto, R. (1999). Regulation of mitochondrial ATP synthesis by calcium: evidence for a long-term metabolic priming. Proc. Natl. Acad. Sci. USA *96*, 13807–13812.

Kawamata, H., Starkov, A.A., Manfredi, G., and Chinopoulos, C. (2010). A kinetic assay of mitochondrial ADP-ATP exchange rate in permeabilized cells. Anal. Biochem. *407*, 52–57.

Keel, S.B., Doty, R.T., Yang, Z., Quigley, J.G., Chen, J., Knoblaugh, S., Kingsley, P.D., De Domenico, I., Vaughn, M.B., Kaplan, J., et al. (2008). A heme export protein is required for red blood cell differentiation and iron homeostasis. Science *319*, 825–828.

Kennedy, J.C., Pottier, R.H., and Pross, D.C. (1990). Photodynamic therapy with endogenous protoporphyrin IX: basic principles and present clinical experience. J. Photochem. Photobiol. B *6*, 143–148.

Khan, A.A., and Quigley, J.G. (2011). Control of intracellular heme levels: heme transporters and heme oxygenases. Biochim. Biophys. Acta *1813*, 668–682.

Kim, H.J., Khalimonchuk, O., Smith, P.M., and Winge, D.R. (2012). Structure, function, and assembly of heme centers in mitochondrial respiratory complexes. Biochim. Biophys. Acta *1823*, 1604–1616.

Kubota, Y., Nomura, K., Katoh, Y., Yamashita, R., Kaneko, K., and Furuyama, K. (2016). Novel mechanisms for heme-dependent degradation of ALAS1 protein as a component of negative feedback regulation of heme biosynthesis. J. Biol. Chem. *291*, 20516–20529.

Lathrop, J.T., and Timko, M.P. (1993). Regulation by heme of mitochondrial protein transport through a conserved amino acid motif. Science *259*, 522–525.

Lee, J., Yesilkanal, A.E., Wynne, J.P., Frankenberger, C., Liu, J., Yan, J., Elbaz, M., Rabe, D.C., Rustandy, F.D., Tiwari, P., et al. (2019). Effective breast cancer combination therapy targeting BACH1 and mitochondrial metabolism. Nature *568*, 254–258.

Luo, F., Brooks, D.G., Ye, H., Hamoudi, R., Poulogiannis, G., Patek, C.E., Winton, D.J., and Arends, M.J. (2009). Mutated K-*ras*^{Asp12} promotes tumourigenesis in *Apc*^{Min} mice more in the large than the small intestines, with synergistic effects between K-*ras* and *Wnt* pathways. Int. J. Exp. Pathol. *90*, 558–574.

Lynch, J.A., Fukuda, Y., Krishnamurthy, P., Wijaya, J., Wang, Y., Herras, A., Cheepala, S., Bao, J., Nourse, A., Milasta, S., et al. (2019). Heme interaction with the pyruvate dehydrogenase complex: a novel strategy to promote hypoxic survival. FASEB J. *33*, 652.12, 652.12.

Malik, Z., and Lugaci, H. (1987). Destruction of erythroleukaemic cells by photoactivation of endogenous porphyrins. Br. J. Cancer *56*, 589–595.

Marchi, S., Corricelli, M., Branchini, A., Vitto, V.A.M., Missiroli, S., Morciano, G., Perrone, M., Ferrarese, M., Giorgi, C., Pinotti, M., et al. (2019). Akt-mediated phosphorylation of MICU1 regulates mitochondrial Ca. EMBO J. *38*, e99435.

Mercurio, S., Petrillo, S., Chiabrando, D., Bassi, Z.I., Gays, D., Camporeale, A., Vacaru, A., Miniscalco, B., Valperga, G., Silengo, L., et al. (2015). The heme exporter Flvcr1 regulates expansion and differentiation of committed erythroid

progenitors by controlling intracellular heme accumulation. Haematologica *100*, 720–729.

Morciano, G., Sarti, A.C., Marchi, S., Missiroli, S., Falzoni, S., Raffaghello, L., Pistoia, V., Giorgi, C., Di Virgilio, F., and Pinton, P. (2017). Use of luciferase probes to measure ATP in living cells and animals. Nat. Protoc. *12*, 1542–1562.

Patron, M., Checchetto, V., Raffaello, A., Teardo, E., Vecellio Reane, D., Mantoan, M., Granatiero, V., Szabò, I., De Stefani, D., and Rizzuto, R. (2014). MICU1 and MICU2 finely tune the mitochondrial $Ca2^+$ uniporter by exerting opposite effects on MCU activity. Mol. Cell *53*, 726–737.

Peng, Q., Moan, J., Warloe, T., Nesland, J.M., and Rimington, C. (1992). Distribution and photosensitizing efficiency of porphyrins induced by application of exogenous 5-aminolevulinic acid in mice bearing mammary carcinoma. Int. J. Cancer *52*, 433–443.

Peng, C., Song, Y., Chen, W., Wang, X., Liu, X., Wang, F., Wu, D., Ma, S., Wang, X., and Gao, C. (2018). FLVCR1 promotes the proliferation and tumorigenicity of synovial sarcoma through inhibiting apoptosis and autophagy. Int. J. Oncol. *52*, 1559–1568.

Petrillo, S., Chiabrando, D., Genova, T., Fiorito, V., Ingoglia, G., Vinchi, F., Mussano, F., Carossa, S., Silengo, L., Altruda, F., et al. (2018). Heme accumulation in endothelial cells impairs angiogenesis by triggering paraptosis. Cell Death Differ. *25*, 573–588.

Quigley, J.G., Yang, Z., Worthington, M.T., Phillips, J.D., Sabo, K.M., Sabath, D.E., Berg, C.L., Sassa, S., Wood, B.L., and Abkowitz, J.L. (2004). Identification of a human heme exporter that is essential for erythropoiesis. Cell *118*, 757–766.

Riganti, C., Gazzano, E., Polimeni, M., Costamagna, C., Bosia, A., and Ghigo, D. (2004). Diphenyleneiodonium inhibits the cell redox metabolism and induces oxidative stress. J. Biol. Chem. *279*, 47726–47731.

Rizzuto, R., Simpson, A.W., Brini, M., and Pozzan, T. (1992). Rapid changes of mitochondrial $Ca2^+$ revealed by specifically targeted recombinant aequorin. Nature *358*, 325–327.

Russo, V., Roperto, F., Taulescu, M., De Falco, F., Urraro, C., Corrado, F., Munday, J.S., Catoi, C., and Roperto, S. (2019). Expression of the feline leukemia virus subgroup C receptors in normal and neoplastic urothelium of the urinary bladder of cattle associated with bovine papillomavirus infection. Vet. Microbiol. *229*, 147–152.

Rutter, J., Winge, D.R., and Schiffman, J.D. (2010). Succinate dehydrogenase—assembly, regulation and role in human disease. Mitochondrion *10*, 393–401.

Sabová, L., Zeman, I., Supek, F., and Kolarov, J. (1993). Transcriptional control of *AAC3* gene encoding mitochondrial ADP/ATP translocator in Saccharomyces cerevisiae by oxygen, heme and ROX1 factor. Eur. J. Biochem. *213*, 547–553.

Sassa, S., and Granick, S. (1970). Induction of δ-aminolevulinic acid synthetase in chick embryo liver cells in cluture. Proc. Natl. Acad. Sci. USA *67*, 517–522.

Schindelin, J., Arganda-Carreras, I., Frise, E., Kaynig, V., Longair, M., Pietzsch, T., Preibisch, S., Rueden, C., Saalfeld, S., Schmid, B., et al. (2012). Fiji: an open-source platform for biological-image analysis. Nat. Methods *9*, 676–682.

Shen, Y., Li, X., Zhao, B., Xue, Y., Wang, S., Chen, X., Yang, J., Lv, H., and Shang, P. (2018). Iron metabolism gene expression and prognostic features of hepatocellular carcinoma. J. Cell. Biochem. *119*, 9178–9204.

Sinclair, P.R., Gorman, N., and Jacobs, J.M. (2001). Measurement of heme concentration. Curr. Protoc. Toxicol., Chapter 8, Unit 8.3.

Srivastava, G., Borthwick, I.A., Maguire, D.J., Elferink, C.J., Bawden, M.J., Mercer, J.F., and May, B.K. (1988). Regulation of 5-aminolevulinate synthase mRNA in different rat tissues. J. Biol. Chem. *263*, 5202–5209.

Stein, P.E., Badminton, M.N., and Rees, D.C. (2017). Update review of the acute porphyrias. Br. J. Haematol. *176*, 527–538.

Vandekeere, S., Dubois, C., Kalucka, J., Sullivan, M.R., García-Caballero, M., Goveia, J., Chen, R., Diehl, F.F., Bar-Lev, L., Souffreau, J., et al. (2018). Serine synthesis via PHGDH Is essential for heme production in endothelial cells. Cell Metab. *28*, 573–587.e13.

Vinchi, F., Ingoglia, G., Chiabrando, D., Mercurio, S., Turco, E., Silengo, L., Altruda, F., and Tolosano, E. (2014). Heme exporter FLVCR1a regulates heme synthesis and degradation and controls activity of cytochromes P450. Gastroenterology *146*, 1325–1338.

Wachowska, M., Muchowicz, A., Firczuk, M., Gabrysiak, M., Winiarska, M., Wanczyk, M., Bojarczuk, K., and Golab, J. (2011). Aminolevulinic acid (ALA) as a prodrug in photodynamic therapy of cancer. Molecules *16*, 4140–4164.

Wan, Q., Dingerdissen, H., Fan, Y., Gulzar, N., Pan, Y., Wu, T.J., Yan, C., Zhang, H., and Mazumder, R. (2015). BioXpress: an integrated RNA-seq-derived gene expression database for pan-cancer analysis. Database (Oxford) *2015*, bav019.

Wang, Y., Nakayama, M., Pitulescu, M.E., Schmidt, T.S., Bochenek, M.L., Sakakibara, A., Adams, S., Davy, A., Deutsch, U., Lüthi, U., et al. (2010). Ephrin-B2 controls VEGF-induced angiogenesis and lymphangiogenesis. Nature *465*, 483–486.

Webber, J., Herman, M., Kessel, D., and Fromm, D. (1999). Current concepts in gastrointestinal photodynamic therapy. Ann. Surg. *230*, 12–23.

Wibom, R., Hagenfeldt, L., and von Döbeln, U. (2002). Measurement of ATP production and respiratory chain enzyme activities in mitochondria isolated from small muscle biopsy samples. Anal. Biochem. *311*, 139–151.

Wiel, C., Le Gal, K., Ibrahim, M.X., Jahangir, C.A., Kashif, M., Yao, H., Ziegler, D.V., Xu, X., Ghosh, T., Mondal, T., et al. (2019). BACH1 stabilization by antioxidants stimulates lung cancer metastasis. Cell *178*, 330–345.e22.

Yamamoto, M., Hayashi, N., and Kikuchi, G. (1982). Evidence for the transcriptional inhibition by heme of the synthesis of delta-aminolevulinate synthase in rat liver. Biochem. Biophys. Res. Commun. *105*, 985–990.

Yamamoto, M., Hayashi, N., and Kikuchi, G. (1983). Translational inhibition by heme of the synthesis of hepatic delta-aminolevulinate synthase in a cell-free system. Biochem. Biophys. Res. Commun. *115*, 225–231.

Yamauchi, K., Hayashi, N., and Kikuchi, G. (1980). Translocation of delta-aminolevulinate synthase from the cytosol to the mitochondria and its regulation by hemin in the rat liver. J. Biol. Chem. *255*, 1746–1751.

Yang, Z., Philips, J.D., Doty, R.T., Giraudi, P., Ostrow, J.D., Tiribelli, C., Smith, A., and Abkowitz, J.L. (2010). Kinetics and specificity of feline leukemia virus subgroup C receptor (FLVCR) export function and its dependence on hemopexin. J. Biol. Chem. *285*, 28874–28882.

Zheng, J., Shan, Y., Lambrecht, R.W., Donohue, S.E., and Bonkovsky, H.L. (2008). Differential regulation of human ALAS1 mRNA and protein levels by heme and cobalt protoporphyrin. Mol. Cell. Biochem. *319*, 153–161.

STAR★METHODS

KEY RESOURCES TABLE

REAGENT or RESOURCE	SOURCE	IDENTIFIER
Antibodies		
Mouse monoclonal, Anti-FLVCR1 (C-4)	Santa Cruz Biotechnology, Dallas, TX USA	Cat#sc-390100
Mouse monoclonal, Anti-ALAS-H (F-5)	Santa Cruz Biotechnology, Dallas, TX USA	Cat#sc-137093; RRID: AB_2225634
Mouse monoclonal, Anti-Vinculin	Sigma Aldrich St. Louis, MO USA	Cat#SAB4200080; RRID: AB_10604160
Rabbit monoclonal, Anti-GAPDH (14C10)	Cell Signaling Technology, Danvers, MA USA	Cat#2118; RRID: AB_561053
Mouse monoclonal, Anti-Firefly Luciferase (CS-17)	Thermofisher Scientific, Waltham, MA USA	Cat# 35-6700, RRID:AB_2533218
Chemicals, peptides, and recombinant proteins		
Collagenase from Clostridium histolyticum, Type I	Sigma Aldrich St. Louis, MO USA	Cat#C0130-500MG
Corning Matrigel Basement Membrane Matrix	Corning Life Sciences, Corning, NY USA	Cat#354234
FITC Annexin 5	Biolegend, San Diego, CA USA	Cat#640906
Propidium iodide solution	Sigma-Aldrich, St. Louis, MO USA	Cat#P4864
Hemin Ferriprotoporphyrin IX chloride	Frontier Scientific, Logan, UT USA	Cat#H651-9
5-Aminolevulinic acid hydrochloride	Sigma Aldrich, St. Louis, MO USA	Cat#A3785
Succinyl-acetone, 4-6 Dioxoheptanoic acid	Sigma Aldrich St. Louis, MO USA	Cat#D1415
PNGase-F from Elizabethkingia meningoseptica	Sigma Aldrich, St. Louis, MO USA	Cat#P-7367
Zn(II) Mesoporphyrin IX	Frontier Scientific, Logan, UT USA	Cat#M40628
Albumin from human serum	Sigma Aldrich, St. Louis, MO USA	Cat#A3782
D-Glucose-$^{13}C_6$	Santa Cruz Biotechnology, Dallas, TX USA	Cat#sc-239643B
L-Glutamine-$^{13}C_5$	Sigma Aldrich, St. Louis, MO USA	Cat#605166
Tamoxifen	Sigma Aldrich St. Louis, MO USA	Cat#T5648
Dulbecco's Phosphate Buffered Saline (DPBS) with Calcium and Magnesium	Lonza Pharma & Biotech, Basel, CH	Cat#BE17-513F
D-Glucose-$^{14}C_6$	PerkinElmer, Waltham, MA, USA	Cat#NEC045X
Palmitic acid-$^{14}C_1$	PerkinElmer, Waltham, MA, USA	Cat#NEC075H
Beetle luciferin, potassium salt (D-luciferin)	Promega, Madison, WI USA	Cat#E1605
Bis-2-(5-phenylacetamido-1,3,4-thiadiazol-2-yl)ethyl sulfide (BPTES)	Sigma Aldrich St. Louis, MO USA	Cat#SML0601
Etomoxir	Sigma Aldrich St. Louis, MO USA	Cat#E1905
5-aminoimidazole-4-carboxamide ribonucleotide (AICAR)	Sigma Aldrich St. Louis, MO USA	Cat#A9978
Coelenterazine, native	Sigma Aldrich St. Louis, MO USA	Cat#C2230
Tetramethylrhodamine methyl ester perchlorate (TMRM)	Sigma Aldrich St. Louis, MO USA	Cat#T5428
JC-1 Dye (Mitochondrial Membrane Potential Probe) (JC-1)	Thermofisher Scientific, Waltham, MA USA	Cat#T3168
Carbonyl cyanide 4-(trifluoromethoxy) phenylhydrazone (FCCP)	Sigma Aldrich St. Louis, MO USA	Cat#C2920
Critical commercial assays		
CD45 MicroBeads, mouse	Miltenyi Biotec, Bergisch Gladbach, DE	Cat#130-052-301
CD31 MicroBeads, mouse	Miltenyi Biotec, Bergisch Gladbach, DE	Cat#130-097-418
CellTiter-Fluor Cell Viability Assay	Promega, Madison, WI USA	Cat#G6080

(*Continued on next page*)

Continued

REAGENT or RESOURCE	SOURCE	IDENTIFIER
Purelink RNA mini kit	Thermofisher Scientific, Waltham, MA USA	Cat#12183018A
High-Capacity cDNA Reverse Transcription Kit	Thermofisher Scientific, Waltham, MA USA	Cat#4368813
Oxaloacetate Assay Kit	Abcam, Cambridge, UK	Cat#ab83428
Citrate Synthase Assay Kit	Sigma Aldrich, St. Louis, MO USA	Cat#MAK193
Alpha Ketoglutarate (alpha KG) Assay Kit	Abcam, Cambridge, UK	Cat#ab83431
Malate Dehydrogenase Assay Kit	Sigma Aldrich, St. Louis, MO USA	Cat#MAK196
Succinate Dehydrogenase Activity Colorimetric Assay Kit	BioVision, Milpitas, CA USA	Cat#K660
ATP Bioluminescent Assay Kit	Sigma-Aldrich, St. Louis, MO USA	Cat#FLAA
Glutamine Synthetase Microplate Assay Kit	Cohesion Biosciences Ltd, London, UK	Cat#CAK102
β-hydroxybutyrate Colorimetric Assay Kit	Cayman Chemical, Ann Arbor, MI USA	Cat#700190
MitoBiogenesis In-Cell ELISA Kit_Colorimetric	Abcam, Cambridge, UK	Cat#ab110217
EndoGRO-MV-VEGF Complete Culture Media Kit	Merck Millipore, Burlington, MA USA	Cat#SCME003
Deposited data		
The Cancer Genome Atlas (TCGA)	https://www.cancer.gov/about-nci/organization/ccg/research/structural-genomics/tcga	N/A
BioXpress	Wan et al., 2015 (https://hive.biochemistry.gwu.edu/bioxpress)	N/A
Experimental models: Cell lines		
SKCO1	ATCC, Manassas, VA USA	Cat#HTB-39; RRID:CVCL_0626
C80	ECACC, Salisbury, UK	Cat#12022904; RRID:CVCL_5249
SHSY-5Y	ATCC, Manassas, VA USA	Cat#CRL-2266; RRID:CVCL_0019
Breast tumor-derived endothelial cells (BTECs)	Grange et al., 2006	N/A
LL/2 (LLC1)	ATCC, Manassas, VA USA	Cat#CRL-1642, RRID:CVCL_4358
Caco2	ATCC, Manassas, VA USA	Cat#HTB-37, RRID:CVCL_0025
Experimental models: Organisms/strains		
Mouse: NSG: NOD.Cg-*Prkdc*^{scid} *Il2rg*^{tm1Wjl}/SzJ	The Jackson Laboratory, Bar Harbor, ME USA	Cat#005557; RRID:IMSR_JAX:005557
Mouse: *Flvcr1a* KO: *Flvcr1a*$^{fl/fl}$;Cdh5-Cre^{ERT2}	This paper	N/A
Mouse: *Flvcr1a*$^{fl/fl}$	Vinchi et al., 2014	N/A
Mouse: Cdh5(PAC)-Cre^{ERT2}: Tg(Cdh5-cre/ERT2)1Rha	Wang et al., 2010	Cat#3848982; RRID:MGI:3848984
Mouse: Apc$^{Min/+}$: C57BL/6J-Apc^{Min}/J	The Jackson Laboratory, Bar Harbor, ME USA	Cat#002020; RRID:IMSR_JAX:002020
Oligonucleotides		
Murine *Cre* Rev: CATCGACCGGTAATGCAG	Vinchi et al., 2014	N/A
Murine *lLoxFlvcr1* Fw: TCTAAGGCCCAGTAGGACCC	Vinchi et al., 2014	N/A
Murine *lLoxFlvcr1* Rev: GAAAGCATTTCCGTCCGCCC	Vinchi et al., 2014	N/A
Murine *llLoxFlvcr1* Rev: AGAGGGCAACCTCGGTGTCC	Vinchi et al., 2014	N/A
Murine *Cre* Fw: ACACCTGCTACCATATCATCCTAC	Vinchi et al., 2014	N/A

(*Continued on next page*)

Continued

REAGENT or RESOURCE	SOURCE	IDENTIFIER
Murine *APC* Rev: TCGTTTATATTCCACTTTGGCATAAGGC	Luo et al., 2009	N/A
Murine *APC* Fw: CAAGTCTGCCATCCCTTCACGTTAGGAA	Luo et al., 2009	N/A
Recombinant DNA		
pLVX-puro empty vector	Clontech Laboratories Inc. A Takara Bio Company, Mountain View, CA, USA	Cat#632164
TRC Lentiviral pLKO.1 Human *FLVCR1* shRNA set, clone TRCN0000059599	Dharmacon, Lafayette, CO, USA	Cat#RHS4533-EG28982
TRC Lentiviral pLKO.1 Human *ALAS1* shRNA set, clone TRCN0000045740 and TRCN0000045738	Dharmacon, Lafayette, CO, USA	Cat#RHS4533-EG211
TRC Lentiviral pLKO.1 Non-targeting Control shRNA	Dharmacon, Lafayette, CO, USA	Cat#RHS6848
pLVX-puro *FLVCR1a* vector	Bertino et al., 2019	N/A
mitochondria-targeted Discosoma sp. red fluorescent protein (mtDsRed)	Gotoh et al., 2004	N/A
mitochondria-targeted GCaMP6m	Patron et al., 2014	N/A
mitochondria-targeted Aequorin (mt-AEQ)	Rizzuto et al., 1992	N/A
mitochondria-targeted Luciferase (mt-LUC)	Jouaville et al., 1999	N/A
Software and algorithms		
BD FACSDIVA software v8.1	BD Biosciences, Milan, IT	https://www.bdbiosciences.com/instruments/software/facsdiva/index.jsp/; RRID:SCR_001456
ProbeFinder software	Roche, Basel, CH	https://lifescience.roche.com/en_it/articles/Universal-ProbeLibrary-System-Assay-Design.html; RRID:SCR_014490
Primer Express software v3.0	Thermofisher Scientific, Waltham, MA USA	https://www.thermofisher.com/order/catalog/product/4363991/; RRID:SCR_014326
Imaris v4.0	Bitplane AG, Zurich, CH	http://www.bitplane.com/imaris/imaris/; RRID:SCR_007370
GraphPad Prism v5.0 and v7.0	GraphPad Software, Inc., La Jolla, CA USA	https://www.graphpad.com/; RRID: SCR_002798
Fiji	Schindelin et al., 2012	https://fiji.sc/; RRID: SCR_002285
Thermo Xcalibur software	Thermofisher Scientific, Waltham, MA USA	https://www.thermofisher.com/order/catalog/product/OPTON-30965#/OPTON-30965
Thermo LCQUAN software	Thermofisher Scientific, Waltham, MA USA	https://www.thermofisher.com/order/catalog/product/LCQUAN25?SID=srch-srp-LCQUAN25#/LCQUAN25?SID=srch-srp-LCQUAN25
Other		
C-SCOPE/CARCINOSCOPE - Absolute Quantitative Analysis of Energy Metabolism	The Human Metabolome Technology, Yamagata, JP	N/A

RESOURCE AVAILABILITY

Lead contact

Further information and requests for resources and reagents should be directed to and will be fulfilled by the lead contact, Emanuela Tolosano (emanuela.tolosano@unito.it).

Materials availability

All unique/stable reagents generated in this study will be made available on request but we may require a payment and/or a completed materials transfer agreement.

Data and code availability

This study did not generate any unique datasets or code.

EXPERIMENTAL MODEL AND SUBJECT DETAILS

Cell lines

Caco2 cells (ATCC, Manassas, VA USA, catalog n° HTB-37, RRID:CVCL_0025) were maintained in Dulbecco's modified Eagle's medium (DMEM, high glucose, GlutaMAX supplement; GIBCO by Thermofisher Scientific, Waltham, MA USA, catalog n°61965059) supplemented with 20% heat-inactivated low-endotoxin fetal bovine serum (FBS; GIBCO by Thermofisher Scientific, Waltham, MA USA, catalog n°10270106), 1 mM Sodium Pyruvate (GIBCO by Thermofisher Scientific, Waltham, MA USA, catalog n°11360039) and 1X MEM Non-essential amino acids solution (GIBCO by Thermofisher Scientific, Waltham, MA USA, catalog n°11140035). SKCO1 (ATCC, Manassas, VA USA, catalog n° HTB-39, RRID:CVCL_0626) were propagated in Minimal essential medium (MEM, GIBCO by Thermo Fisher Scientific, Waltham, MA USA, catalog n°21090022) supplemented with 10% heat-inactivated low-endotoxin FBS (GIBCO by Thermofisher Scientific, Waltham, MA USA, catalog n°10270106) and 2mM L-glutamine (Thermo Fisher Scientific, Waltham, MA USA, catalog n°25030024). C80 cells (ECACC, Salisbury, UK catalog n° 12022904, RRID:CVCL_5249) were maintained in Iscove's modified Dulbecco's medium (IMDM, GlutaMAX supplement; GIBCO by Thermo Fisher Scientific, Waltham, MA USA, catalog n°31980022), supplemented with 10% heat-inactivated low-endotoxin FBS (GIBCO by Thermofisher Scientific, Waltham, MA USA, catalog n°10270106). SHSY-5Y cells (ATCC, Manassas, VA USA, catalog n° CRL-2266, RRID:CVCL_0019) were maintained in Dulbecco's Modified Eagle Medium Nutrient Mixture F-12 (DMEM-F12, GIBCO by Thermo Fisher Scientific, Waltham, MA USA, catalog n°31330038) supplemented with 10% heat-inactivated low endotoxin FBS (GIBCO by Thermofisher Scientific, Waltham, MA USA, catalog n°10270106). BTECs (Grange et al., 2006) were maintained in EndoGRO-MV-VEGF Complete Culture Media Kit (Merck Millipore, Burlington, MA USA, catalog n° SCME003). LL/2 (LLC1) cells (ATCC, Manassas, VA USA, catalog n° CRL-1642, RRID:CVCL_4358) were cultured in Dulbecco's modified Eagle's medium (DMEM, high glucose, GlutaMAX supplement; GIBCO by Thermofisher Scientific, Waltham, MA USA, catalog n° 61965059) supplemented with 10% heat-inactivated low-endotoxin fetal bovine serum (FBS; GIBCO by Thermofisher Scientific, Waltham, MA USA, catalog n°10270106).

All cell media were ordinarily supplemented with antibiotics (100U/ml penicillin and 100μg/ml streptomycin; GIBCO by Thermo Fisher Scientific, Waltham, MA USA, catalog n°15140122). Cells were maintained in a 37°C and 5% CO_2 air incubator and routinely screened for absence of mycoplasma contamination.

Animal models

Transgenic $Apc^{Min/+}$ mice were from The Jackson Laboratory (Bar Harbor, ME USA; C57BL/6J-Apc^{Min}/J, catalog n°002020, RRID:IMSR_JAX:002020).

For genotyping, primers Apc-Fw (5′ CAAGTCTGCCATCCCTTCACGTTAGGAA 3′) and Apc-Rev (5′ TCGTTTATATTCCACTTTGGCATAAGGC 3′) (Luo et al., 2009) were used to amplify the portion of *Apc* gene containing the Apc^{Min} mutation (a transversion point mutation that alters nucleotide 2549 in *Apc* mRNA: NM_001360980.1 from a T to an A, converting codon 850 from one encoding a leucine to a stop codon). The obtained DNA was then sequenced to discriminate mice for the presence of the mutated allele. Tumors were collected in different tracts of the intestine of 17-week-old males.

NOD SCID gamma (NSG) mice were from The Jackson Laboratory (Bar Harbor, ME USA; NOD.Cg-*Prkdc*^{scid} *Il2rg*^{tm1Wjl}/SzJ, catalog n°005557, RRID: IMSR_JAX:005557). 8-week-old males were used for the experiments.

Tamoxifen-inducible endothelial specific *Flvcr1a* null mice (*Flvcr1a*$^{fl/fl}$;Cdh5(PAC)-Cre^{ERT2} mice, named *Flvcr1a*-KO in the text and figures) were generated in our laboratory. Briefly, previously generated *Flvcr1a*$^{fl/fl}$ mice (Vinchi et al., 2014) were crossed with Cdh5(PAC)-Cre^{ERT2} mice (Tg(Cdh5-cre/ERT2)1Rha, MGI ID: 3848982, RRID:MGI:3848984) (Wang et al., 2010), kindly provided by Ralf H. Adams, on a C57BL/6 background. Mice were genotyped by polymerase chain reaction (PCR) analyses on DNA from tail biopsies. To detect the Cdh5-Cre allele, primers Cre-Fw (5′ ACA CCT GCT ACC ATA TCA TCC TAC 3′) and Cre-Rev (5′ CAT CGA CCG GTA ATG CAG 3′) were used. To analyze the LoxP sites on *Flvcr1* gene, primers ILox-Fw (5′-TCTAAGGCCCAGTAGGACCC-3′) and ILox-Rev (5′-GAAAGCATTTCCGTCCGCCC-3′) were used, given a 280-bp band for the floxed allele and a 242-bp band for the wild-type allele. To inactivate *Flvcr1a* selectively in endothelial cells, 6-week-old Flvcr1a$^{fl/fl}$;Cdh5(PAC)-Cre^{ERT2} males were treated intraperitoneally with 1mg/day tamoxifen (Sigma Aldrich St. Louis, MO USA, catalog n°T5648) for 3 consecutive days, followed by 3 additional days after a 4-days treatment free interval. To detect the *Flvcr1a* null allele resulting from Cdh5-Cre activity, primers ILox-Fw (5′-TCTAAGGCCCAGTAGGACCC-3′) and IILox-Rev (5′-AGAGGGCAACCTCGGTGTCC-3′) were used, given a 320-bp fragment. Tamoxifen-treated *Flvcr1a*$^{fl/fl}$ mice were used as control.

All the mice were provided with food and water *ad libitum*. Experiments were performed on males.

All experiments with animals were approved by the Italian Ministry of Health.

METHOD DETAILS

Analyses on human samples databases

The frequency of tumors showing upregulated *FLVCR1* expression with respect to their matched normal tissue was determined using the online tool BioXpress (Wan et al., 2015) (https://hive.biochemistry.gwu.edu/bioxpress). Only those samples that have matched normal tissue expression data were used for this analysis. Numbers of patients overexpressing *FLVCR1* in tumor relative to total number of patients examined for that tumor subtype are indicated in the figure. A binomial test was performed to assess the statistical significance of the number of patients overexpressing *FLVCR1* in tumor relative to the total number of patients for that tumor subtype, the null hypothesis being equal probability of *FLVCR1* being up or downregulated in cancer for each patient.

In silico determination of FLVCR1 gene expression in colon adenocarcinoma and rectum adenocarcinoma human samples was also performed by a direct analysis on data reported in The Cancer Genome Atlas (TCGA). In this case, for the evaluation of FLVCR1 expression in human tumors and matched normal tissues, 41 and 8 primary colon and rectum tumors, respectively, were analyzed. A paired Wilcoxon test was performed to assess the statistical significance of the difference in expression.

Gene silencing and overexpression

FLVCR1a silencing was performed as described in Destefanis et al. (2019). Briefly, different shRNAs for the human *FLVCR1* transcripts were tested. We selected the only one which specifically downregulates *FLVCR1a*, without targeting the FLVCR1b isoform (TRC Lentiviral pLKO.1 Human *FLVCR1* shRNA set RHS4533-EG28982, clone TRCN0000059599; Dharmacon, Lafayette, CO, USA).

To specifically downregulate *ALAS1*, two different shRNAs targeting the human *ALAS1* transcript were used (TRC Lentiviral pLKO.1 Human *ALAS1* shRNA set RHS4533-EG211, clone TRCN0000045740, named shRNA *ALAS1* in the figure, and TRCN0000045738, named shRNA $ALAS1_2$ in the figure; Horizon Discovery, Cambridge, UK).

For control cells, a pLKO.1 lentiviral vector expressing a scramble shRNA (TRC Lentiviral pLKO.1 Non-targeting Control shRNA, catalog n° RHS6848; Dharmacon, Lafayette, CO, USA) was used.

Gene overexpression was performed as described in Bertino et al. (2019). Briefly, the *FLVCR1a* cDNA present in pCMV-SPORT6 vector (MGC human FLVCR1 sequence, clone 4417876, Horizon Discovery, Cambridge, UK, catalog n° MHS6278-202757940) and the Myc-tag sequence present in pcDNA3.1(-)/myc-His B (Thermofisher Scientific, Waltham, MA USA, catalog n° V85520) were cloned in frame in the pLVX-puro vector, a lentiviral expression vector with constitutively active human cytomegalovirus immediate early promoter and the puromycin resistance gene (Clontech Laboratories Inc. A Takara Bio Company, Mountain View, CA, USA, catalog number 632164), in order to obtain the pLVX-puro *FLVCR1a* vector. For control cells, a pLVX-puro empty vector (Clontech Laboratories Inc. A Takara Bio Company, Mountain View, CA, USA, catalog number 632164) was used.

Following lentiviral transduction, cells were maintained in selective medium containing 0.002mg/ml puromycin (Puromycin dihydrochloride from *Streptomyces alboniger*, Sigma-Aldrich, St. Louis, MO USA, catalog n° P8833).

Tumor-associated endothelial cells isolation

Tumor-associated endothelial cells (TECs) were isolated from Lewis lung carcinoma xenografted subcutaneous tumors in tamoxifen-inducible endothelial specific *Flvcr1a* null mice (*Flvcr1a*$^{fl/fl}$;Cdh5(PAC)-Cre^{ERT2} mice, named *Flvcr1a*-KO in the text and figures) or control (*Flvcr1a*$^{fl/fl}$) mice. Briefly, tumors were dissected and minced into 1–2mm fragments with a scalpel. Tissue pieces were incubated at 37°C for 60 minutes in 10mL of pre-warmed Dulbecco's Phosphate Buffered Saline (DPBS) with Calcium and Magnesium (Lonza Pharma & Biotech, Basel, CH, catalog n° BE17-513F) and 2mg/ml Collagenase (Collagenase from Clostridium histolyticum, Type I, Sigma Aldrich St. Louis, MO USA, catalog n°C0130), with regular shacking until a single cell suspension was obtained. During this incubation, the cells were mechanically dissociated at 10minutes intervals by pipetting. To stop the collagenase activity, DMEM (GIBCO by Thermofisher Scientific, Waltham, MA USA, catalog n° 61965059) containing 10% FBS (GIBCO by Thermofisher Scientific, Waltham, MA USA, catalog n°10270106) was added to the cell suspension, gently pelleted, and rinsed with PBS. The cells in PBS were then filtered through a 40μm Cell Strainer (Corning Life Sciences, Corning, NY USA, catalog n°352340). Single-cell suspension was centrifuged at 300 x *g* for 10 minutes and tumor-associated endothelial cells were isolated through MACS Technology by using nano-sized MicroBeads, following the manufacturer instructions. Particularly, a negative selection was performed using CD45 MicroBeads (Miltenyi Biotec, Bergisch Gladbach, DE, catalog n°130-052-301). CD45-negative cell fraction was then pelleted and incubated with CD31 MicroBeads (Miltenyi Biotec, Bergisch Gladbach, DE, catalog n°130-097-418) to obtain endothelial cells.

Xenograft tumor model

For the SKCO1 xenograft model, 8-week-old NOD SCID gamma (NSG) mice (The Jackson Laboratory, Bar Harbor, ME USA; NOD.Cg-*Prkdc*^{scid} *Il2rg*^{tm1Wjl}/SzJ, catalog n° 005557, RRID: IMSR_JAX:005557) were housed in a temperature-controlled, pathogen-free environment and used for experimentation. The mice were randomly divided into two groups (n = 6 per group). $5*10^6$ SKCO1 cells, stably expressing a shRNA to *FLVCR1a* or to a scramble control sequence, were suspended in a solution 50%v/v of PBS and matrigel (Corning Matrigel Basement Membrane Matrix, Corning Life Sciences, Corning, NY USA, catalog n° 354234) and then subcutaneously injected into the right flank of mice. After 11 weeks, mice were sacrificed and tumors were harvested. Tumor length (L) and width (W) were measured and tumor volume (mm^3) was calculated using the following formula: $(L \times W^2)/2$.

For the Lewis lung carcinoma xenograft model, $5x10^5$ LL/2 (LLC1) (ATCC: CRL-1642) murine cells suspended in 100μl PBS were injected subcutaneously into the flanks of immunocompetent syngeneic (C57BL/6) tamoxifen-inducible endothelial specific *Flvcr1a* null mice (*Flvcr1a*$^{fl/fl}$;Cdh5(PAC)-Cre^{ERT2} mice, named *Flvcr1a*-KO in the text and figures) or control (*Flvcr1a*$^{fl/fl}$) mice. Both control and inducible knockout mice were treated intraperitoneally with tamoxifen (Sigma Aldrich St. Louis, MO USA, catalog n°T5648; 1mg/day for 3 consecutive days and 3 additional days after a 4-days treatment free interval) one week before cancer cell injection.

All experimental procedures were approved by the Italian Ministry of Health.

Hematoxylin and eosin staining

Following harvesting, the tissue was washed with 0.1M phosphate-buffered saline (PBS). After overnight fixation in 4% formaldehyde at 4°C, the tissue was decalcified in 0.25M EDTA pH = 7.7 for several days and then embedded in paraffin. 5μm-thick paraffin sections were stained with hematoxylin and eosin (H&E) following standard procedures.

Cell viability assay

To assess cell viability, the CellTiter-Fluor Cell Viability Assay (Promega, Madison, WI USA, catalog n°G6080) was used. The assay is based on measurement of a conserved and constitutive protease activity within live cells and therefore serves as a biomarker of cell viability unrelated to mitochondrial function. The detection of cell viability at different consecutive time points was regarded as a readout of cell proliferation.

Crystal Violet staining

For crystal violet staining, $1*10^4$ Caco2 cells were seeded in 6-well plates. Staining was performed at different time points for each cell group in triplicate. Before staining, cells were washed in 0.1M PBS, fixed in 4% paraformaldehyde for 10 minutes. After PFA removal, a 0.1% crystal violet (Sigma-Aldrich, St. Louis, MO USA) solution was applied for 10 minutes under room temperature. The plates were rinsed with water until non color came off and then dried overnight at room temperature. Stained area was assessed by analyses of four representative photos per day for each triplicate using Fiji open source software (Schindelin et al., 2012) (https://fiji.sc/; RRID:SCR_002285).

Apoptosis analysis

For cell apoptosis analyses, cells were synchronized in appropriate medium containing 0.1% FBS. The day after, serum was re-introduced. 48h hours after serum supplement, $5*10^5$ cells were collected, washed in PBS, resuspended in 10mM HEPES, 140mM NaCl, 2.5mM CaCl2 buffer, and labeled with FITC Annexin 5 (Biolegend, San Diego, CA USA, catalog n°640906) for 20 minutes. Then, 2μl of propidium iodide (1mg/ml) (propidium iodide solution 1mg/ml in water, Sigma-Aldrich, St. Louis, MO USA, catalog n° P4864) was added.

Stained cells were analyzed using a FACSCanto II cytofluorimeter and processed with BD FACSDIVA Software v8.1 (BD Biosciences, Milan, IT; https://www.bdbiosciences.com/instruments/software/facsdiva/index.jsp/; RRID:SCR_001456), acquiring at least 10,000 events per sample or 25,000 cells per sample for cell cycle experiments.

Hemin, 5-ALA and SA cell treatment

Hemin (Hemin Ferriprotoporphyrin IX chloride, Frontier Scientific, Logan, UT USA, catalog n° H651-9) was freshly prepared by dissolution in cell culture-grade Dimethyl sulfoxide (DMSO, Sigma Aldrich, St. Louis, MO USA, catalog n°276855) at a concentration of 4mM and then diluted in tissue culture medium at a concentration of 25μM.

5-ALA (5-Aminolevulinic acid hydrochloride, Sigma Aldrich, St. Louis, MO USA, catalog n°A3785) was freshly prepared by dissolution in tissue culture medium at a concentration of 5mM.

SA (Succinyl-acetone, 4-6 Dioxoheptanoic acid, Sigma Aldrich St. Louis, MO USA, catalog n°D1415) was freshly prepared by dissolution in tissue culture medium at a concentration of 0.5mM.

All solutions were kept in the dark.

RNA extraction and quantitative real-time PCR analysis

RNA extraction and quantitative real-time PCR analyses were performed as described previously (Destefanis et al., 2019). Briefly, total RNA was extracted using Purelink RNA mini kit (Thermofisher Scientific, Waltham, MA USA, catalog n° 12183018A). Between 500 and 1000ng of total RNA were transcribed into complementary DNA (cDNA) by High-Capacity cDNA Reverse Transcription Kit (Thermofisher Scientific, Waltham, MA USA, catalog n° 4368813). Quantitative real-time PCR (qRT-PCR) was performed using the Universal Probe Library system (Roche, Basel, CH). Primers and probes were designed using the ProbeFinder software (Roche, Basel, CH, https://lifescience.roche.com/en_it/articles/Universal-ProbeLibrary-System-Assay-Design.html; RRID:SCR_014490). For *FLVCR1a* and *FLVCR1b*, specific primers and the probe were designed using Primer Express Software v3.0 (Thermofisher Scientific, Waltham, MA USA, https://www.thermofisher.com/order/catalog/product/4363991/; RRID:SCR_014326). qRT-PCR were performed on a 7300 or 7900 Real Time PCR System (Thermofisher Scientific, Waltham, MA USA). Transcript abundance, normalized to *18 s* mRNA expression (for mouse tissues, mouse TECs and for BTECs) or to beta-actin mRNA expression (for cells, except TECs and BTECs), is expressed as a fold increase over a calibrator sample.

Western blot analysis

To assess FLVCR1a and ALAS1 expression, cells were lysed by rotation for 30 minutes at 4°C in RIPA buffer (150mM NaCl, 50mM Tris-HCl pH 7.5, 1% Triton X-100, 0.5% Sodium deoxycholate, 0.1% SDS, 1mM EDTA). The buffer was freshly supplemented with 1mM phosphatase inhibitor cocktail (Sigma Aldrich, St. Louis, MO USA, catalog n° P0044), 1mM PMSF (Sigma Aldrich, St. Louis, MO USA, catalog n° 93482-50ML-F) and protease inhibitor cocktail (Roche, Basel, CH, catalog n° 04693116001). The cell lysate was clarified by centrifugation for 10 minutes at 4°C. Protein concentration in the supernatant was assessed by Bradford assay. For FLVCR1a detection, to remove protein glycosylation, 10μg of protein extracts were incubated 10 minutes at 37°C with 1μL of PNGase-F from Elizabethkingia meningoseptica (Sigma Aldrich, St. Louis, MO USA, catalog n° P-7367). Before loading on 4%–15% mini-PROTEAN TGX precast gel (Bio-Rad, Hercules, CA USA, catalog n°4568084), samples were incubated 5 minutes at 37°C (for FLVCR1a detection) or 5 minutes at 95°C (for ALAS1 detection) in 4X laemmli buffer freshly supplemented with 8% 2-mercaptoethanol. The primary antibodies and dilutions are as follows: mouse monoclonal anti-FLVCR1 (C-4) (Santa Cruz Biotechnology, Dallas, TX USA, catalog n° sc-390100; 1:500), mouse monoclonal anti-ALAS-H (F5) (Santa Cruz Biotechnology, Dallas, TX USA, catalog n° sc-137093; RRID: AB_2225634; 1:1000) and mouse monoclonal anti-Vinculin (Sigma Aldrich, St. Louis, MO USA, catalog n° SAB4200080; RRID: AB_10604160, 1:8000). The revelation was assessed using the ChemiDoc Imaging System (Bio-Rad, Hercules, CA USA).

To assess luciferase expression, cells were lysed on ice for 30 minutes in a buffer containing 50mM Tris-HCl pH 7.4, 150mM NaCl, 1% Triton X-100, 0.2% SDS, protease, and phosphatase inhibitor cocktail. The cell lysate was clarified by centrifugation and 30 μg of proteins were loaded on a Bis-Tris 4%–12% precast gel (Thermofisher Scientific, Waltham, MA USA). The primary antibodies and dilutions are as follows: rabbit monoclonal anti-GAPDH (14C10) (Cell Signaling Technology, Danvers, MA USA, catalog n° 2118; RRID:561053; 1:5000) and mouse monoclonal anti-Firefly Luciferase (CS-17) (Thermofisher Scientific, Waltham, MA USA, 35-6700; RRID:2533218; 1:500). The revelation was assessed using ImageQuant LAS 4000 (GE Healthcare, Chicago, IL, USA).

Zinc-mesoporphyrin washout experiments

Zinc-Mesoporphyrin (ZnMP) export studies were performed, as described previously (Yang et al., 2010), by preloading cells for 30 minutes at 37°C with 5μM ZnMP (Zn(II) Mesoporphyrin IX, Frontier Scientific, Logan, UT USA, catalog n°M40628) dissolved in cell culture-grade Dimethyl sulfoxide (DMSO, Sigma Aldrich St. Louis, MO USA, catalog n°276855) at a concentration of 4mM and then diluted to 5μM in working buffer (25mM HEPES (pH 7.4), 130mM NaCl, 10mM KCl, 1mM $CaCl_2$, and 1mM $MgSO_4$) freshly supplemented with 2.5μM Albumin from human serum (HSA, Sigma Aldrich, St. Louis, MO USA, catalog n°A3782). Cells were then washed once with ice-cold working buffer containing 5% bovine serum albumin (BSA), and twice with ice cold working buffer, in order to remove the excess ZnMP not internalized by cells. Acquired intracellular fluorescence was determined on a Glomax Multi Detection System (Promega Corporation, Madison WI, USA) with excitation at 405nm and emission at 580-640nm, upon lysis in TBS 1X-Triton X-100 1%. Concomitantly, matched cell samples were washed three times and incubated in working buffer with 5μM HSA for 60 minutes at 37°C to promote ZnMP export (washout phase).

After cells lysis in TBS 1X-Triton X-100 1%, samples residual intracellular fluorescence was determined on a Glomax Multi Detection System (Promega Corporation, Madison WI, USA) with excitation at 405nm and emission at 580-640nm. Data were normalized to total protein concentration in each sample. All experimental steps were performed in the dark. ZnMP retention was expressed as the percentage residual intracellular fluorescence, measured upon washout, with respect to the starting fluorescence, detected immediately after the uptake phase, in ZnMP loaded matched samples.

Measurement of heme concentration

Intracellular heme concentration was measured using a fluorescence assay, as previously reported (Sinclair et al., 2001). Briefly, cells untreated or treated for different times with 5-ALA or SA were collected and 2M oxalic acid was added to them. Samples were heated at 95°C for 30 minutes leading to iron removal from heme. Fluorescence (wavelength: excitation 405nm - emission 660-720nm) of the resultant protoporphyrin was assessed on a Glomax Multi Detection System (Promega Corporation, Madison WI, USA).

The endogenous protoporphyrin content (measured in parallel unheated samples in oxalic acid) was subtracted. Data were normalized to total protein concentration in each sample. Results were expressed as relative fluorescence intensity or, alternatively, as pmol of heme/mg total protein.

Metabolome analysis

Metabolome analysis (C-SCOPE/CARCINOSCOPE - Absolute Quantitative Analysis of Energy Metabolism) was performed by The Human Metabolome Technology (Yamagata, JP).

Assessment of metabolites levels

The levels of metabolites, except oxaloacetate, were determined by metabolome analyses (C-SCOPE/CARCINOSCOPE - Absolute Quantitative Analysis of Energy Metabolism, The Human Metabolome Technology, Yamagata, JP) and expressed as μmol/g cellular proteins. The levels of oxaloacetate were measured by the Oxaloacetate Assay Kit (Abcam, Cambridge, UK, catalog n° ab83428), as per manufacturer's instructions, and expressed as μmol/mg cellular proteins.

NAD+ and NADH levels assessment

The levels of NAD+ and NADH were determined by metabolomic analyses (C-SCOPE/CARCINOSCOPE - Absolute Quantitative Analysis of Energy Metabolism, The Human Metabolome Technology, Yamagata, JP) and expressed as μmoles/g cellular proteins.

^{13}C-isotope labeling experiments

FLVCR1a-silenced and scramble shRNA-expressing cells were plated in six-well plates in 25mM glucose, 4mM glutamine and 1mM pyruvate-containing DMEM (DMEM, high glucose, pyruvate; GIBCO by Thermofisher Scientific, Waltham, MA USA, catalog n°11995-065) supplemented with 10% FBS at 3x10^5 cells per well. After 24 hours the medium was replaced with 10% FBS- and 1mM pyruvate-supplemented DMEM containing 4mM unlabelled glutamine (DMEM, no glucose; GIBCO by Thermofisher Scientific, Waltham, MA USA, catalog n°11966-025) and 25mM $^{13}C_6$-glucose (D-Glucose-$^{13}C_6$, Santa Cruz Biotechnology, Dallas, TX USA, catalog n° sc-239643B) for $^{13}C_6$-glucose-tracing experiments; alternatively, the medium was replaced with 10% FBS-supplemented DMEM containing 25mM unlabelled glucose (DMEM, high glucose, pyruvate, no glutamine, GIBCO by Thermofisher Scientific, Waltham, MA USA, catalog n°21969-035) and 4mM $^{13}C_5$-glutamine (L-Glutamine-$^{13}C_5$, Sigma Aldrich, St. Louis, MO USA, catalog n°605166), for $^{13}C_5$-glutamine tracing experiments. The labeled medium was maintained for time indicated in each figure caption. At the end of the incubations, monolayers were rapidly washed three times with ice-cold PBS and extracted with 600μl of ice-cold extraction solution, composed of methanol, acetonitrile and Milli-Q water (5:3:2), for endo-metabolite determination. Cell extracts were centrifuged at 16,000 x *g* for 20 minutes at 4°C and the supernatants were analyzed by liquid chromatography-mass spectrometry (LC-MS). An Exactive Orbitrap mass spectrometer (Thermofisher Scientific, Waltham, MA USA) was used together with a Thermo Scientific Accela HPLC system. The HPLC setup consisted of a ZIC-pHILIC column (SeQuant, 150mm × 2.1mm, 5μm, Merck KGaA, Darmstadt, DE) with a ZIC-pHILIC guard column (SeQuant, 20mm × 2.1mm, Merck KGaA, Darmstadt, DE) and an initial mobile phase of 20% 20mM ammonium carbonate, pH 9.4 and 80% acetonitrile. Cell extracts (5μl) were injected and metabolites were separated over a 15-minutes mobile phase gradient, decreasing the acetonitrile content to 20%, at a flow rate of 200 μL min^{-1} and a column temperature of 45°C. The total analysis time was 23 minutes. All metabolites were detected across a mass range of 75-1,000 m/z using the Exactive mass spectrometer at a resolution of 25,000 (at 200 m/z), with electrospray ionization and polarity switching. Lock masses were used and the mass accuracy obtained for all metabolites was below 5p.p.m. Data were acquired with Thermo Xcalibur software (Thermofisher Scientific, Waltham, MA USA, https://www.thermofisher.com/order/catalog/product/OPTON-30965#/OPTON-30965). The peak areas of different metabolites were determined with Thermo LCQUAN software (Thermofisher Scientific, Waltham, MA USA, https://www.thermofisher.com/order/catalog/product/LCQUAN25?SID=srch-srp-LCQUAN25#/LCQUAN25?SID=srch-srp-LCQUAN25), identified by the exact mass of each singly charged ion and by the known retention time on the HPLC column, obtained by running commercial standards of all metabolites detected. The ^{13}C labeling patterns were determined by measuring peak areas for the accurate mass of each isotopologue of several metabolites. Peak areas of each metabolite were normalized to the protein content in each well measured, at the end of the experiment, using the Lowry assay.

Mitochondria isolation

According to Wibom et al. (2002), cells were washed twice in ice-cold 0.1M phosphate-buffered saline (PBS), then lysed in 0.5mL buffer A (50mmol/L Tris, 100mmol/L KCl, 5mmol/L $MgCl_2$, 1.8mmol/L ATP, 1mmol/L EDTA, pH 7.2), supplemented with protease inhibitor cocktail III [100 mmol/L AEBSF, 80mmol/L aprotinin, 5mmol/L bestatin, 1.5mmol/L E-64, 2mmol/L leupeptin and 1mmol/L pepstatin (Merck KGaA, Darmstadt, DE)], 1mmol/L phenylmethylsulfonyl fluoride (PMSF), 250mmol/L NaF. Samples were clarified by centrifuging at 650 x *g* for 3 minutes at 4°C, and the supernatant was collected and centrifuged at 13,000 x *g* for 5 minutes at 4°C. The new supernatant was discarded, the pellet containing mitochondria was washed in 0.5mL buffer A and re-suspended in 0.25mL buffer B (250mmol/L sucrose, 15 μmol/L K_2HPO_4, 2mmol/L $MgCl_2$, 0.5mmol/L EDTA, 5% w/v bovine serum albumin). A 100 μL aliquot was sonicated and used for the measurement of protein content and the enzymatic activities of citrate synthase, α-ketoglutarate dehydrogenase, succinate dehydrogenase and malate dehydrogenase. The remaining not-sonicated part was used to measure the electron transport chain (ETC) complexes I-IV activities.

Citrate synthase, α-ketoglutarate dehydrogenase, succinate dehydrogenase and malate dehydrogenase activities

The enzymatic activities of citrate synthase, α-ketoglutarate dehydrogenase, succinate dehydrogenase and malate dehydrogenase were measured on 10μg mitochondrial proteins using the Citrate Synthase Assay Kit (Sigma Aldrich, St. Louis, MO USA, catalog n° MAK193), Alpha Ketoglutarate (alpha KG) Assay Kit (Abcam, Cambridge, UK, catalog n° ab83431), Malate Dehydrogenase Assay Kit (Sigma Aldrich, St. Louis, MO USA, catalog n° MAK196), Succinate Dehydrogenase Activity Colorimetric Assay Kit (BioVision, Milpitas, CA USA, catalog n° K660), as per manufacturer's instructions. Results were expressed as mU/mg mitochondrial proteins.

Activity of mitochondrial ETC complexes I-IV

The activity of mitochondria respiration complexes was measured according to Wibom et al. (2002).

Oxygen consumption rate measurement

Oxygen consumption rate (OCR) was measured with a XF^{e}96 Extracellular Flux Analyzer (Seahorse Bioscience, Billerica, MA, USA) in 10^4 cells/well. The growth medium was replaced with 180 μL of bicarbonate-free DMEM supplemented with 10mM glucose, 2mM

L-glutamine and 1mM sodium pyruvate pre-warmed at 37°C. After measuring basal respiration, Oligomycin (1 μM), carbonyl cyanide-4 (triluoromethoxy) phenylhydrazone (FCCP, 0.8 μM), and rotenone (1 μM) + antimycin A (1 μM) were injected into each well sequentially to assess respectively coupling of respiratory chain, maximal and non-mitochondrial oxygen consumption. OCR values were normalized to protein content in each well, determined with BCA assay.

Measurement of total cellular ATP levels

Total cellular ATP levels were determined by metabolomic analyses (C-SCOPE/CARCINOSCOPE - Absolute Quantitative Analysis of Energy Metabolism, The Human Metabolome Technology, Yamagata, JP) and expressed as μmoles/g cellular proteins.

Measurements of cytosolic ATP levels

The cytosolic ATP level was determined using a luciferase-based method as previously described (Morciano et al., 2017). Cells were transfected with cytosolic-targeted luciferase encoding plasmid. After 36 hours, cells were perfused with KRB buffer, supplemented with 1mM $CaCl_2$ and 20mM D-luciferin (Beetle luciferin, potassium salt, Promega, Madison, WI USA, catalog n°E1605). The luminescence values obtained upon addiction of luciferin correspond to the amount of ATP in the cytosolic compartment.

ATP levels in mitochondria and activity of mitochondrial ATP-synthase

Mitochondrial ATP levels were measured using a luciferase probe targeted to the mitochondrial matrix (mt-LUC) (Jouaville et al., 1999; Morciano et al., 2017). Cells were perfused with KRB buffer, supplemented with 1mM $CaCl_2$ and 20mM D-luciferin (Beetle luciferin, potassium salt, Promega, Madison, WI USA, catalog n°E1605) (plateau I). To evoke ATP production, cells were perfused with the same luciferin solution plus 100 μM ATP (plateau II). Basal mitochondrial ATP content (plateau I) and mitochondrial ATP levels after Ca^{2+}-dependent stimulation (plateau II) were expressed as luminescence values.

The activity of mitochondrial ATP-synthase was indirectly assessed measuring the accumulation of mitochondrial ATP over the basal ATP levels, upon stimulation of ATP synthesis (plateau II - plateau I).

Alternatively, ATP levels in mitochondria extracts were assessed by the ATP Bioluminescent Assay Kit (Sigma-Aldrich, St. Louis, MO USA, catalog n° FLAA). In this case, ATP was quantified as relative light units (RLU) and converted into nmol ATP/mg mitochondrial proteins, according to the calibration curve previously set.

Adenine nucleotide translocases (ANTs) activity

The activity of ANTs was measured fluorimetrically on 250μg mitochondrial proteins according to Kawamata et al. (2010). Results were expressed as μmoles exchanged ATP/mg mitochondrial proteins.

Tricarboxylic acid (TCA) cycle flux

The glucose flux through TCA cycle was measured by radiolabeling cells with 2 μCi/ml [6-^{14}C]-glucose (55mCi/mmol; PerkinElmer, Waltham, MA, USA, catalog n° NEC045X). Cell suspensions were incubated for 1 hour in a closed experimental system to trap the $^{14}CO_2$ developed from [^{14}C]-glucose. The reaction was stopped by injecting 0.5ml of 0.8N $HClO_4$. The amount of glucose transformed into CO_2 through the TCA cycle was calculated as described (Riganti et al., 2004) and expressed as pmoles CO_2/h/mg cell proteins.

Glutaminase (GLS) and glutamine synthetase (GLUL) activity

Glutamine catabolism was measured as reported (Curthoys and Weiss, 1974), with minor modifications, as detailed in Capello et al. (2016). Briefly, cells were washed with PBS, detached by gentle scraping, centrifuged at 13,000 x *g* for 5 minutes at 4°C, re-suspended in 250μL of buffer A (150mmol/L KH_2PO_4, 63mmol/L Tris/HCl, 0.25mmol/L EDTA; pH 8.6) and sonicated. A volume of 100μL of the whole cell lysates was incubated for 30 minutes at 37°C in a quartz cuvette, in the presence of 50μL of 20mmol/L L-glutamine and 850μL of buffer B (80mmol/L Tris/HCl, 20mmol/L NAD^+, 20mmol/L ADP, 3% v/v H_2O_2; pH 9.4). The absorbance of NADH was monitored at 340nm using a Lambda 3 spectrophotometer (PerkinElmer, Waltham, MA USA). The kinetics was linear throughout the assay. The results were expressed as μmol NADH/min/mg cell proteins, and were considered as an index of the activity of glutaminase (GLS) plus L-glutamic dehydrogenase (GLUDH). In a second series of samples, 20μL of the 30μmol/L GLS inhibitor bis-2-(5-phenylacetamido-1,3,4-thiadiazol-2-yl) ethyl sulfide (BPTES, Sigma Aldrich St. Louis, MO USA, catalog n° SML0601) was added after 15 minutes. This concentration was chosen as it produced 100% inhibition of GLS activity in our system (not shown). The absorbance of NADH was monitored for 15 minutes as described previously. The results, considered as an index of the activity of GLUDH, were expressed as μmol NADH/min/mg cell proteins. GLS activity was obtained by subtracting the rate of the second assay from the rate of the first one.

The enzymatic activity of glutamine synthetase (GLUL) was measured spectrophotometrically, using the Glutamine Synthetase Microplate Assay Kit (Cohesion Biosciences Ltd, London, UK, catalog n° CAK102). Results were expressed as mU/mg cellular proteins.

Fatty acids β-oxidation measurement

The rate of palmitic acid oxidation, considered an index of fatty acid β-oxidation, was measured by metabolic radiolabeling in whole cell lysates as reported in Gaster et al. (2004). Briefly, cells were washed twice with PBS, detached with trypsin/EDTA

(0.05/0.02% v/v) and centrifuged at 13,000 x *g* for 5 minutes. A 50μL aliquot was collected, sonicated and used for intracellular protein quantification. The remaining sample was re-suspended in culture medium containing 0.24mmol/L fatty acid-free bovine serum albumin, 0.5mmol/L L-carnitine, 20mmol/L HEPES, 2μCi [1-^{14}C] palmitic acid (3.3mCi/mmol, PerkinElmer, Waltham, MA USA, catalog n° NEC075H) and transferred into test tubes that were tightly sealed with rubber caps. In each experimental set cells were pre-incubated for 30 minutes with the carnitine palmitoyltransferase inhibitor etomoxir (1μmol/L, Sigma Aldrich St. Louis, MO USA, catalog n° E1905) or with the AMP-kinase activator 5-aminoimidazole-4-carboxamide ribonucleotide AICAR (1mmol/L, Sigma Aldrich St. Louis, MO USA, catalog n° A9978), as negative and positive controls, respectively. After 2 hours incubation at 37°C, 0.3mL of a 1:1 v/v phenylethylamine/methanol solution was added to each sample using a syringe, followed by 0.3mL 0.8N $HClO_4$. Samples were incubated for a further 1 hour at room temperature, then centrifuged at 13,000 x *g* for 10 minutes. Both the supernatants, containing $^{14}CO_2$, and the precipitates, containing ^{14}C-acid soluble metabolites (ASM), were collected. The radioactivity of each sample was counted by liquid scintillation. Results were expressed as pmol of [$^{14}CO_2$], used as internal control, or ^{14}C-ASM/h/mg cell proteins. In each experimental set, the amount of [$^{14}CO_2$] was always < 10% than the amount of ^{14}C-ASM.

Ketone bodies measurement

The amount of β-hydroxybutyrate, taken as an index of ketone bodies amount, was assessed in the whole cell lysate using the β-hydroxybutyrate Colorimetric Assay Kit (Cayman Chemical, Ann Arbor, MI USA, catalog n° 700190). Results were expressed as μmoles/mg cellular proteins.

The amount of β-hydroxy-β-methylglutaryl-CoA was determined by metabolomic analyses (C-SCOPE/CARCINOSCOPE - Absolute Quantitative Analysis of Energy Metabolism, The Human Metabolome Technology, Yamagata, JP) and expressed as μmoles/g cellular proteins.

Mitochondrial biogenesis

Mitochondrial biogenesis was detected with the MitoBiogenesis In-Cell ELISA Kit_Colorimetric (Abcam, Cambridge, UK, catalog n° ab110217).

Additionally, parameters describing the mitochondrial network dynamics were measured, including number of mitochondrial objects, total mitochondrial volume and mean volume of single mitochondrial object. Control and *FLVCR1a*-silenced Caco-2 cells were seeded and transfected with mitochondria-targeted Discosoma sp. red fluorescent protein (mtDsRed) (Gotoh et al., 2004) to specifically mark the mitochondrial compartment. Protein expression was allowed for 36 hours and then cells were imaged with the same microscope used for measurements of membrane potential. 21 planes with 0.6 μm distance z stacks were acquired to allow acquisition of the whole cell. After acquisition, images were restored with the Autoquant 3D-blind deconvolution module, installed on NIS-Elements (Nikon Instruments Inc.), using a theoretical PSF. After restoration, images were loaded in Imaris v4.0 (Bitplane AG, Zurich, CH, http://www.bitplane.com/imaris/imaris/; RRID:SCR_007370) then subtracted of background, and used to generate a threshold-based isosurface object group.

Mitochondrial basal calcium levels measurement

The mitochondrial basal calcium levels were determined as described in Marchi et al. (2019). Briefly, cells were grown on 24mm coverslips and transfected with mitochondrial-targeted GCaMP6m (mt- GCaMP6m) encoding plasmid (Patron et al., 2014; Marchi et al., 2019). Imaging was performed on Cell^Sense multiple wavelength high-resolution fluorescence microscopy system, using a 40x objective. Cells were alternatively illuminated at 474 and 410nm and fluorescence was collected through a 515/30nm band pass filter. Analysis was performed with the Fiji open source software (Schindelin et al., 2012) (https://fiji.sc/; RRID:SCR_002285). Data are presented as the mean of the averaged ratio of all time points.

Mitochondrial calcium uptake measurement

The mitochondrial calcium uptake was determined as previously described (Bonora et al., 2013). Briefly, cells were seeded onto 13mm glass coverslips and transfected with a mitochondrial-targeted Aequorin probe (mt-AEQ) (Rizzuto et al., 1992; Bonora et al., 2013). Before the measurement, cells were incubated with 5 μM coelenterazine for 1.5 hour in KRB buffer supplemented with 1mM $CaCl_2$, and then transferred to the perfusion chamber. Cells were stimulated using IP3-dependent agent (ATP 100 μM) in order to evoke Ca^{2+} discharge from the Endoplasmic Reticulum and rapid Ca^{2+} accumulation inside mitochondria. The experiments were terminated by lysing cells with Triton X-100 in a hypotonic Ca^{2+}-rich solution, thus discharging the remaining aequorin pool. The light signal was collected and calibrated into [Ca^{2+}] values by an algorithm based on the Ca^{2+} response curve of aequorin at physiological conditions of pH, [Mg^{2+}], and ionic strength.

Mitochondrial membrane potential measurements

Mitochondrial membrane potential was measured by the Tetramethylrhodamine, methyl ester (TMRM) fluorescent dye-based method. Cells were loaded with 20nM Tetramethylrhodamine methyl ester perchlorate (TMRM, Sigma Aldrich St. Louis, MO USA, catalog n° T5428) for 30 minutes at 37°C. Successively, cells were imaged with Nikon Swept Field Confocal equipped with CFI Plan Apo VC60XH objective (n.a. 1.4) and an Andor DU885 EM-CCD camera, controlled by the NIS-Elements 3.2. Basal levels

were normalized on fluorescence in the presence of Carbonyl cyanide 4-(trifluoromethoxy)phenylhydrazone (FCCP, Sigma Aldrich St. Louis, MO USA, catalog n° C2920).

Additionally, the data were confirmed measuring mitochondrial membrane potential by the JC-1 fluorescent dye-based method (JC-1 Dye_Mitochondrial Membrane Potential Probe, Thermofisher Scientific, Waltham, MA USA, catalog n° T3168) on a high throughput system (Olympus ScanˆR system). Cells were loaded with 25 μM JC-1 for 30 minutes at 37°C, and then automatically imaged using a 20x objective. The ratio of red to green fluorescence has been reported.

QUANTIFICATION AND STATISTICAL ANALYSIS

Sample size, mean and statistical details of experiments can be found in the figure legends.

Statistical analyses were conducted in GraphPad Prism v5.0 and v7.0 (GraphPad Software, Inc., La Jolla, CA USA, https://www.graphpad.com/; RRID:SCR_002798), or reported by the computational tools. No statistical method was used to predetermine sample size in studies.